JOURNAL OF QUATERNARY SCIENCE (2003) **18**(6) 527–543

Published online 24 July 2003 in Wiley InterScience (www.interscience.wiley.com). DOI: 10.1002/jqs.771

Glaciotectonised Quaternary sediments at Cape Shpindler, Yugorski Peninsula, Arctic Russia: implications for glacial history, ice movements and Kara Sea Ice Sheet configuration

HANNA LOKRANTZ,[1]* ÓLAFUR INGÓLFSSON[2] and STEVEN L. FORMAN[3]
[1] Geological Survey of Sweden, Villavägen 18, Box 670, SE-751 28 Uppsala, Sweden
[2] Department of Geology and Geography, University of Iceland, IS-101 Reykjavík, Iceland
[3] Department of Earth and Environmental Sciences, University of Illinois at Chicago, 845 W. Taylor Street, Chicago, IL 60607-7059, USA

Lokrantz, H., Ingólfsson, Ó. and Forman, S. L. 2003. Glaciotectonised Quaternary sediments at Cape Shpindler, Yugorski Peninsula, Arctic Russia: implications for glacial history, ice movements and Kara Sea Ice Sheet configuration. *J. Quaternary Sci.*, **Vol. 18** pp. 527–543. ISSN 0267-8179.

Received 14 March 2002; Revised 25 February 2003; Accepted 21 March 2003

ABSTRACT: The coastal cliffs of Cape Shpindler, Yugorski Peninsula, Arctic Russia, occupy a key position for recording overriding ice sheets during past glaciations in the Kara Sea area, either from the Kara Sea shelf or the uplands of Yugorski Peninsula/Polar Urals. This study on Late Quaternary glacial stratigraphy and glaciotectonic structures of the Cape Shpindler coastal cliffs records two glacier advances and two ice-free periods older than the Holocene. During interglacial conditions, a sequence of marine to fluvial sediments was deposited. This was followed by a glacial event when ice moved southwards from an ice-divide over Novaya Zemlya and overrode and disturbed the interglacial sediments. After a second period of fluvial deposition, under interstadial or interglacial conditions, the area was again subject to glacial overriding, with the ice moving northwards from an inland ice divide. The age-control suggests that the older glacial event could possibly belong to marine oxygen isotope stage (MOIS) 8, Drenthe (300–250 ka), and that the underlying interglacial sediments might be Holsteinian (>300 ka). One implication of this is that relict glacier ice, buried in sediments and incorporated into the permafrost, may survive several interglacial and interstadial events. The younger glacial event recognised in the Cape Shpindler sequence is interpreted to be of Early-to-Middle Weichselian age. It is suggested to correlate to a regional glaciation around 90 or 60 ka. The Cape Shpindler record suggests more complex glacial dynamics during that glaciation than can be explained by a concentric ice sheet located in the Kara Sea, as suggested by recent geological and model studies. Copyright © 2003 John Wiley & Sons, Ltd.

KEYWORDS: Arctic Russia; Kara Sea; Yugorski Peninsula; Pleistocene; glacial history; lithostratigraphy; massive ground ice; glaciotectonism; chronology; ^{14}C; OSL.

Introduction

Northern Russia, western Siberia and adjacent wide shelf areas were repeatedly glaciated during the Pleistocene (Astakhov, 1994; Svendsen *et al.*, 1999; Thiede *et al.*, 2001). However, contradicting hypotheses are proposed for ice-sheet geometries, including locations of ice divides and limits and age for various ice-sheet configurations (Arkhipov *et al.*, 1986; Astakhov, 1992, 1994; Rutter, 1995; Svendsen *et al.*, 1999). Cape Shpindler, on the Yugorski Peninsula (Fig. 1a and b), occupies a key position for recording the passage of overriding ice-sheets that originated on Novaya Zemlya and flowed across the Kara Sea shelf, and also for ice-caps that originated in the highlands of the Ural Mountains or Pai-Hoi uplands of Yugorski Peninsula and dispersed ice seawards. Stratigraphical data from this area that constrain past glacier movements have been scarce. Goldfarb *et al.* (1985) were first to describe the coastal cliffs at Cape Shpindler. They recorded Quaternary marine, lagoonal, fluvial, deltaic and glacial deposits, which were interpreted to record two glaciations and three interglacials and/or interstadials. Stratigraphical studies by Manley *et al.* (2001) confirm the occurrence of two interglacial–interstadial events. That study also observed opposing directions of glacial push from the

* Correspondence to: Dr Hanna Lokrantz, Geological Survey of Sweden, Villavägen 18, Box 670, SE-751 28 Uppsala, Sweden. E-mail: hanna.lokrantz@sgu.se

Contract/grant sponsor: Swedish Natural Sciences Research Council.
Contract/grant sponsor: YMER.

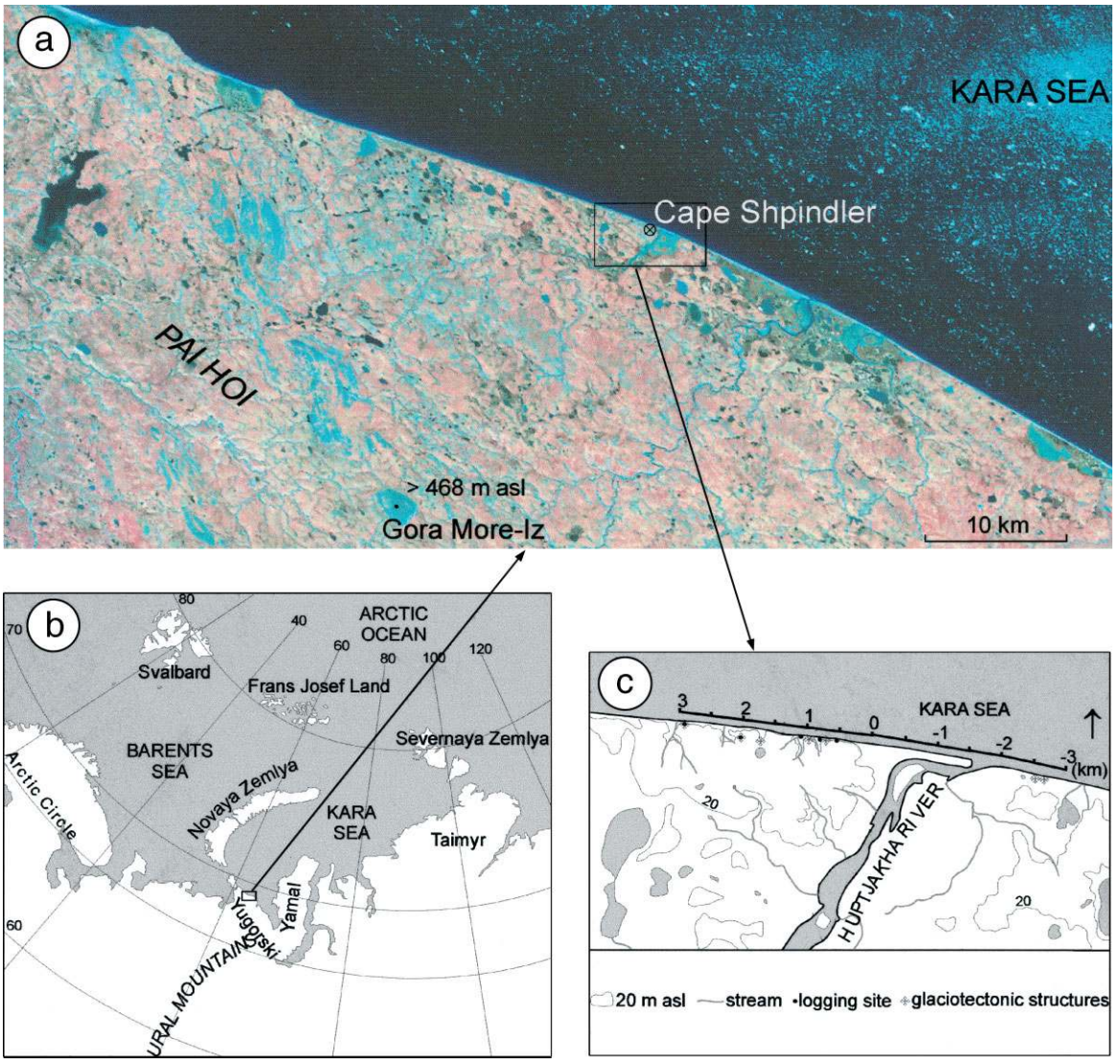

Figure 1 Location maps of the coastal sections studied at Cape Shpindler. (a) A regional map of Yugorski Peninsula in the form of a LANDSAT image; (b) Eurasia; (c) location of the sections studied

north and the south, from source areas on Novaya Zemlya and from a marginal ice-cap on the Pai Hoi uplands or the Polar Urals, respectively. However, the sequencing of the two inferred advances was unclear because the two glacial diamictons were not observed in stratigraphical superposition. Manley *et al.* (2001) speculated that ice push from the north preceded movement from the south. Both glacial advances are pre-dated by infinite AMS ^{14}C ages on associated organics from the sequence (≥40 kyr BP) and post-dated by such from 12.5 kyr BP, and Manley *et al.* (2001) suggested that the lowermost interglacial sediments were of Eemian age (MOIS (marine oxygen isotope stage) 5e) and that the sequence possibly recorded two Weichselian episodes of glacial deposition.

This paper reports new litho- and chronostratigraphical data collected at Cape Shpindler in the summer of 1999. The focus of this field research was to better document the stratigraphical position of glacial deposits and associated glaciotectonic structures in the sections. These observations are critical for enhancing reconstructions of Late Pleistocene glacial history of northern Eurasia and provide new insights on glacier dynamics, such as basal thermal regime and stress fields. The lithostratigraphical, chronostratigraphical and glaciotectonic data from Cape Shpindler build on the previously presented stratigraphy of Manley *et al.* (2001) but have new implications for ice-sheet nucleation and geometries.

Setting

Cape Shpindler is located north of the uplands of Pai-Hoi (Fig. 1a and b), at the mouth of Huptjakha River and along the Kara Sea coast (Fig. 1c). The Pai-Hoi uplands are a northwest continuation of the Polar Urals. South of Cape Shpindler, the Pai-Hoi uplands rise to approximately 200 m a.s.l., with peak elevations of 468 m a.s.l. at Gora More-Iz, and the bedrock consists of Permian arenaceous–argillaceous strata with coal-bearing deposits. Bedrock structures trend north-northwest to south-southweast, and the general alignment of the Pai Hoi range is approximately west-northwest to east-southeast (Fig. 1a). Bedrock exposures are lacking along the coastal sections of Cape Shpindler.

Cape Shpindler and its immediate surroundings are characterised by alternating shallow valleys and higher ground (Figs. 1a and c), trending west-northwest to east-southeast, where higher ground appears to coincide with the occurrence of massive ground-ice. Massive ground-ice is widely distributed in the southern Kara Sea area and is variously interpreted as relict glacier ice (Kaplayanskaya and Tarnogradsky, 1986; Astakhov and Isayeva, 1988; Astakhov *et al.*, 1996) and/or segregation ice (Mahaney *et al.*, 1995; Michel, 1998). Coastal erosion at Cape Shpindler has resulted in coastal cliffs 15 to 50 m high, trending

approximately east-southeast to west-northwest. Moreover, coastal erosion and nivation processes have eroded the massive ground-ice, forming a number of thermocirques with steep sides, which provide excellent exposures of the stratigraphy.

Methods

Sections and heights of coastal cliff faces were measured by hand levelling and barometric altimeters, using the present high tide beach-level as reference. Longer distances along the cliffs were estimated by repeated GPS measurements. Stratigraphical relationships were examined between different sedimentological units in the coastal cliffs and contacts between different lithostratigraphical units were traced along the cliffs in order to assess unit geometries and to construct schematic cross-sections. Detailed sedimentological logging was conducted, emphasising lithology, grain size, structures and bed and unit contacts to identify the different lithologic units, and to propose interpretations of the different depositional processes and environments. Field observations focused on delineating glaciotectonic structures and related glacial deposits, to interpret former directions of ice movement and basal glacier conditions. Glaciotectonic structural measurements are reported following the right-hand rule, and plotted in the lower hemisphere of stereographic Schmidt nets. Age control is provided for the stratigraphy by AMS radiocarbon dating of wood and a mammoth bone at Ångströmslaboratoriet at Uppsala, Sweden and by optically stimulated dating of polymineral and quartz extracts from selected sediments at the Luminescence Dating Research Laboratory, University of Illinois at Chicago.

Stratigraphy

We investigated a 3.3 km stretch of coastal cliffs west of the Huptjakha River mouth, with the cliff closest to the river as the zero kilometredatum (Fig. 1c). The lithostratigraphy is presented by five logs (Figs 1c and 2) and a schematic cross-section (Fig. 3), in which eight stratigraphical units were discerned, and are as follows from oldest to youngest:

Unit A: marine diamicton

Unit A is the lowermost exposed stratigraphical unit at Cape Shpindler. It is a dark grey, silty clayey and matrix-supported diamicton, usually massive but occasionally laminated. Between 2.0 and 2.9 km in the section, unit A reaches 1 to 3 m a.s.l. (Fig. 2, log 2.9 km; Fig. 3). Its lower contact is not exposed. West of 2.9 km (Fig. 3) its upper contact occurs at approximately 5 m a.s.l. The upper contact of unit A reaches a maximum elevation of more than 20 m a.s.l. east of 1.8 km (Fig. 3). Unit A contains non-striated bedrock clasts, often occurring in clusters, and small intraclasts of sand and silt with their primary stratification preserved. Subfossil twigs, burrows, Foraminifera and molluscs are ubiquitous. The mollusc fauna includes *Macoma calcarea, Nuculana minuta, Mytilus edulis, Ciliatocardium ciliatum and Balanus crenatus*. Foraminifera are well preserved in the sediments, and are dominated by *Buccella frigida*, *Elphidium excavatum* and *Islandiella helenae*. The mollusc fauna lacks warm boreal indicators and together with the foraminiferal taxa suggest that unit A is a shallow marine deposit, deposited in a sub-arctic environment with open marine conditions, potentially similar to present conditions.

Unit B: pro-deltaic silt and mud

Unit B is exposed between 1.7 and 3.3 km and 0.4 and 0.7 km (Fig. 2, logs 0.61 km and 2.9 km; Fig. 3) and contains a lithofacies association of cross-stratified gravelly sand and beds of laminated silt and sand. It predominantly shows vertical variations in grain size, which is most distinct at 2.9 km (Fig. 2) where the unit attains a total thickness of approximately 5 m. Here, cross-stratified gravelly sand fills channels eroded into unit A, with overlying cross-stratified to planar parallel-stratified sandy beds. There is a fining upward trend in the lithofacies: beds of ripple-laminated and planar laminated silts, with a tendency towards hummocky cross-stratification and intercalated with clay seams, grade into massive to laminated silty clay at the top of the unit. Individual beds are normally graded and become thinner upwards. Unit B at approximately 2.0 km consists of 5-cm-thick, alternating beds of medium sand and silt with *in situ* articulated shells of *Nuculana minuta*. Unit B, at 0.5 and 0.6 km and in the lower part at 2.9 km, is dominated by ca. 20-cm-thick beds of cross-stratified gravelly sand, where the orientation of cross-stratification (190° to 205°; inclined 4° to 35°; Fig. 2, logs 0.61 km and 2.9 km) could indicate a palaeocurrent direction from the east-southeast.

The paired molluscs of *Nuculana minuta* indicate shallow-water marine deposition. A plausible interpretation is that Unit B was deposited subaqueously, with periodic input of channelised stream water. The upwards fining and thinning beds could represent decreasing energy due to a lateral shift of the source of stream water in an estuarine or prodeltaic environment with periodicity in energy, possibly in connection with a regression. Palaeocurrent directions, interpreted from the orientation of cross-beds, and the coarsening trend from west to east, could suggest a sediment input from an easterly direction.

Unit C: delta/floodplain sand and silt

Unit C occurs along almost the entire section studied and constitutes the bulk of the sediments (Fig. 3). It sometimes reaches a thickness of >20 m. The lower contact of this unit is sharp and conformable. It undergoes a lateral lithofacies change from west to east and is divided into two subunits, C1 and C2.

Subunit C1 is exposed at 3.3 km and eastwards to approximately 1.7 km (Fig. 2, log 2.9 km; Fig. 3) as alternating beds of ripple-laminated fine sand and mud. A 15-cm-thick layer of cross-stratified and massive, well-sorted medium sand defines the boundary between unit B and overlying unit C1, at the 2.9 km section. Thin beds of silt and mud, with lenticular, wavy and flaser bedding, dominate the lower part of the subunit at 2.9 km. Upwards, unit C1 mainly consists of alternating 20 to 50 cm beds of ripple-laminated coarse silt to fine sand and crudely laminated silty clay. Alternating beds of ripple-laminated sand and laminated mud is the dominant lithofacies of unit C1. In the western wall of the bluffs, west of the gully at 1.8 km, peat mats were observed in the sandy beds. East of the gully, subunit C1 grades into the sandier subunit C2.

Subunit C2 occurs mainly between sections 0.2 and 0.8 km (Figs 2 and 3). At 0.61 km (Fig. 2) subunit C2 constitutes a fining

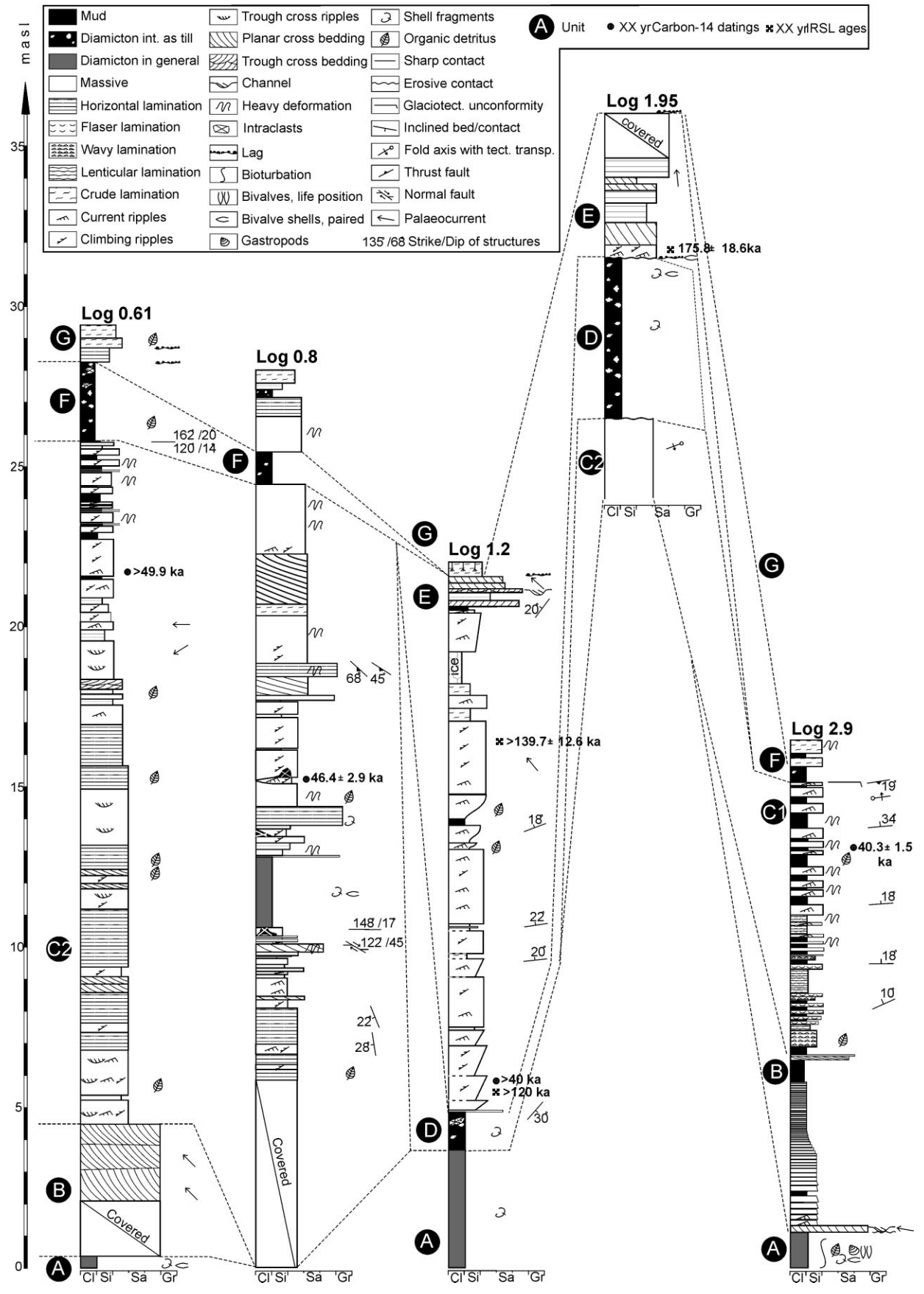

Figure 2 Lithostratigraphical logs of the Cape Shpindler coastal sections. Sites for the logs are marked in Figs 1c and 3

upward sequence with planar parallel-laminated and trough cross-ripple-laminated medium sand dominating the lower part of the subunit and alternating beds of ripple-laminated fine sand and mud in its upper part. Detrital organics occur often in the ripple foresets, and one planar parallel-laminated sand bed holds abundant macrosized remains of rootlets and moss. Orientation of ripple foresets may indicate a palaeocurrent direction from the east.

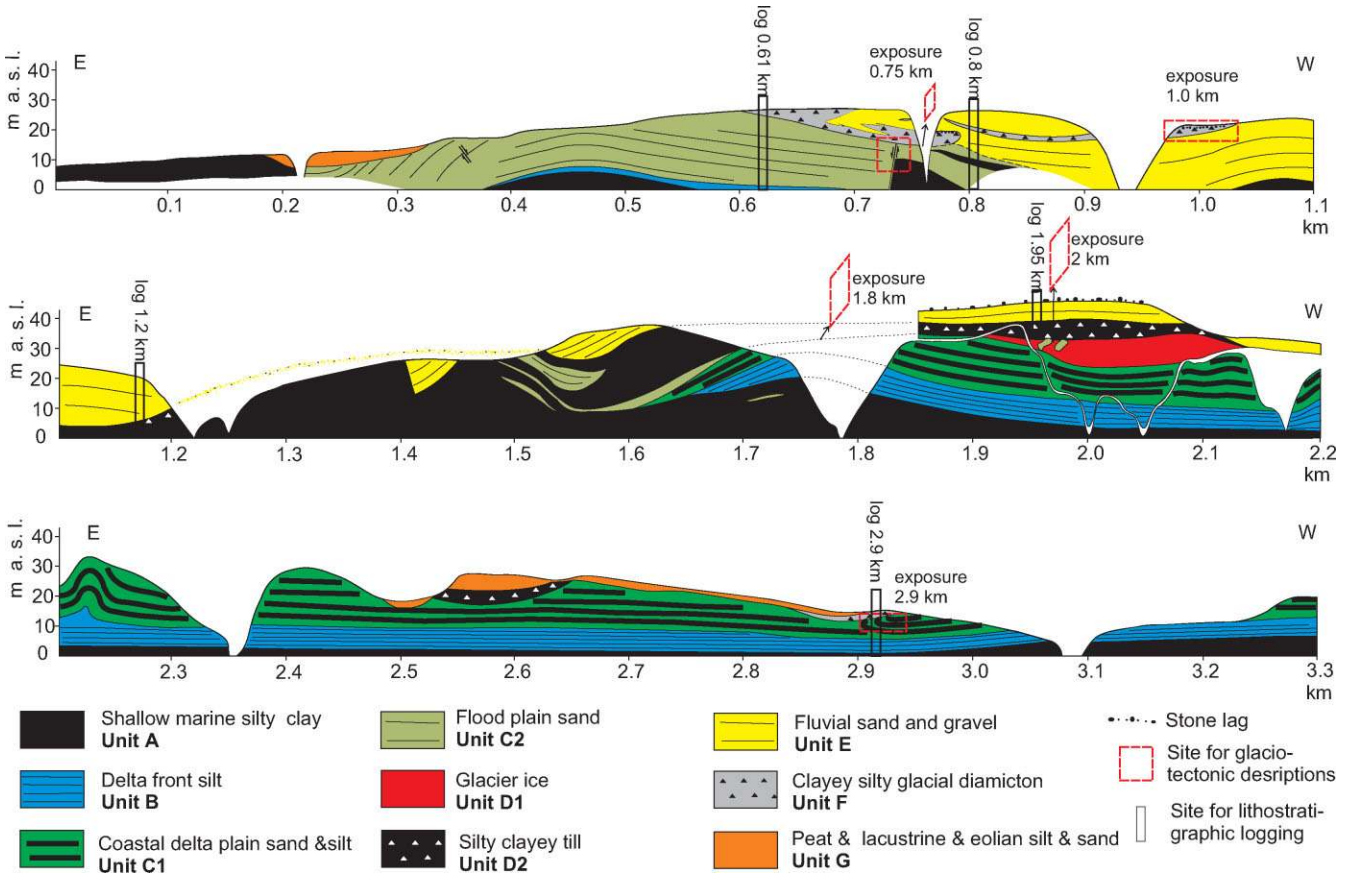

Figure 3 Stratigraphical profile west of Huptjakha river mouth, across the Cape Shpindler coastal cliffs

Unit C is interpreted to represent a low-gradient deposition, in a coastal plain–delta association (C1) and a floodplain association (C2; cf. Reineck and Singh, 1975). Specifically, C1and C2 sediments were deposited in a tidal flat setting, and in shallow fluvial channel and overbank environment, respectively. Moss and vascular detritus from both subunits yielded AMS radiocarbon ages >40 ka BP (Table 1; Manley *et al.*, 2001).

The succession from marine to fluviodeltaic environments in units A through C reflects a base-level fall either reflecting increasing sediment supply and/or a fall in relative sea-level, potentially resulting from regional glacio-isostatic unloading. Environmental conditions for this sedimentological succession with its documented marine fauna probably occurred during interstadials or early within interglacials during the past 700 ka. We tentatively suggest that units A–C were deposited under interglacial conditions, based on the similarity of the molluscan fauna of unit A to the recent one.

Unit D: glacial ice/till complex

Unit D is a complex of massive ground-ice and a clayey diamicton. It is divided into two subunits, D1 and D2. Subunit D1 is composed of massive ground-ice, exposed in the thermocirque between 1.9 and 2.1 km (Fig. 3). The ice body reaches a thickness of >10 m and has a sharp lower contact. The ice consists of alternating layers of bubbleous, transparent and laminated muddy ice. It is contorted and deformed into folds, both upright and isoclinal recumbent, with amplitudes ranging from decimetres to metres. Furthermore, the ice contains 3 to 5 m large intraclasts of folded sand strata.

Subunit D2 is a dark grey, clayey, massive and matrix-supported diamicton and occurs between 1.8 and 2.1 km in the thermocirque area and conspicuously at the 1.2 and 2.6 km sections (Fig. 2, logs 1.2 km and 1.95 km; Fig. 3). This unit attains a thickness of up to 8 m in the thermocirque at 2 km where it is superimposed on the massive ground-ice of subunit D1. In the eastern wall the banding in the ice continues into the diamicton. Elsewhere, the lower contact of subunit D2 to subunit D1 and unit C sediments is sharp and unconformable. Underlying unit C shows evidence of both brittle and ductile deformation, and in places is a glaciotectonite (Benn and Evans, 1996; see below). The diamicton of subunit D2 is dense and firm, and contains paired shells, single valves and fragments throughout. Striated and bullet-shaped clasts were observed in the sections at 1.2 and 1.95 km. Deformed intraclasts of sand occur in the eastern wall of the thermocirque within unit D and bridge the two subunits. The deformed intraclasts define imbricated folds on the scale of 1-to-3-m, verging southwards (see below), with sharp contacts to the surrounding ice and sediments.

Bullet-shaped bedrock clasts and deformed intraclasts of sand indicate that unit D2 is a glacial diamicton. Stratified and foliated ice, unconformably overlain by glacigenic sediments, is indicative of glacier ice (French and Harry, 1990) and unit D1 is interpreted to be buried relict glacier ice. The intraclasts of sand are interpreted as glaciotectonically transported allochthons of unit C. The superposition of the glacial diamicton and its contacts to the relict glacier ice indicate that the diamicton and sand rafts originated from a basal part of a glacier and were subsequently thrusted to an englacial or supraglacial position (cf. Astakhov *et al.*, 1996; Hambrey *et al.*, 1999). Thus, the glacial diamicton cover served to preserve the glacier ice. The occurrence of whole valves and shell fragments indicates that marine sediments, presumably from the Kara Sea, were one source of material for the glacial diamicton.

Table 1 AMS ^{14}C dates from Cape Shpindler. Dates marked with * and ** are from Manley *et al.* (2001) and Andreev *et al.* (2001), respectively

Unit/km	Metres above sea-level	Dated material	Sample number	Laboratory number	^{14}C yr BP $\pm 1\ \sigma$
G/−3.3	10.9	Plant macrofossils		AA-35453**	2580 ± 45
G/−3.5	10.4	Plant macrofossils		AA-35452**	3955 ± 55
G/−3.5	8.9	Woody twig		AA-31387**	5030 ± 55
G/2.55	25.7	Plant macrofossils	CS98-05:1.00*	AA-31378	5415 ± 50
G/0.31	13.1	Plant macrofossils	CS98-12D*	AA-31391	5710 ± 60
G/2.55	27.2	Plant macrofossils	CS98-05:2.50*	AA-31379	5900 ± 50
G/−3.5	7.5	Plant macrofossils		AA-35451**	6830 ± 55
G/2.55	25.4	Plant macrofossils	CS98-05:0.70*	AA-31377	7070 ± 80
G/−3.5	6.8	Plant macrofossils		AA-35450**	8270 ± 60
G/1.0	25.7	Plant macrofossils	CS98-04:2.06*	AA-31376	8305 ± 60
G/−3.85	5.85	Plant macrofossils		AA-35449**	9290 ± 65
G/−3.85	4.2	Plant macrofossils		AA-35447**	9470 ± 65
G/−3.85	4.6	Plant macrofossils		AA-31386**	9670 ± 95
G/1.0	24.2	Woody twigs	CS98-04:0.50*	AA-31375	10 675 ± 75
G/0.22	5.6	Woody twigs	CS98-06:5.60*	AA-31380	11 880 ± 85
G/−3.85	3.8	Plant macrofossils		AA-31385**	12 500 ± 85
G/−3.85	3.5	Plant macrofossils		AA-35446**	12 780 ± 80
G/−3.85	5.2	Plant macrofossils		AA-35448**	12 830 ± 80
E/0.9	12	Mammoth rib	CS99-9	Ua-15356	>40 000
E/1.2	6	Wood	CS99-8	Ua-15355	>40 000
E/2.0	40	Wood	CS99-2	Ua-15353	>40 000
E/2.0	45	Wood (log)	CS993	Ua-15354	>40 000
C1/2.9	13	Plant macrofossils	CS98-07F*	AA-31381	40 306 ± 1537
D1/2.1	30	Plant macrofossils	CS98-15A*	AA-31393	44 000 ± 2200
D1/2.1	30	Plant macrofossils	CS98-15B*	AA-31394	44 500 ± 2300
C2/0.8	15.2	Plant macrofossils	CS98-14A*	AA-31392	46 400 ± 2900
C2/0.6	21.7	Plant macrofossils	CS98-03E*	AA-31374	>49 900

Unit E: fluvial sand

Unit E was observed between 1.8 and 2.2 km in the coastal cliffs and it was traced eastward as a surface cover on the coastal plateau, behind the cliffs, to 1.2 km; from there it occurs in the bluffs to 0.65 km (Fig. 3). Unit E is a lithofacies association of cross-stratified gravelly sand, planar parallel-laminated sand, massive sand and ripple cross-laminated sand and silt (Fig. 2, logs 1.2 km and 1.95 km; Fig. 4). Charcoal, twigs and larger pieces of wood occur occasionally within the unit. Manley *et al.* (2001) chose to consider this unit as an allochthon of unit C. Our new results distinguish unit E from unit C on the basis of its stratigraphical position above unit D glacial diamicton in the thermocirque, and because unit E is exposed between the glacial diamictons of units D and F (see below) between 1.0 and 1.2 km (Fig. 3). Its lower contact to unit D is sharp and unconformable.

In the thermocirque section, around 2 km, unit E attains a maximum thickness of 10 m. There, it is mainly composed of cross-stratified medium sand and gravel, with secondary occurrence of ripple cross-laminated and planar parallel-laminated sand (Fig. 2, log 1.95 km; Fig. 4a). Orientations of cross-bedding indicate palaeocurrent directions from the south-east (Fig. 4a).

Unit E reaches a maximum thickness of 25 m between 0.9 and 1.2 km in the section. There it is composed of 1 to 2 m thick beds of ripple cross-laminated fine sand (Fig. 2, log 1.2 km; Fig. 4b). These beds are primarily inversely graded with silt in the lower parts. Inversely graded to normally graded beds occur less frequently and are bounded at the bottom and the top by a thin bed of clayey silt or mud. This lithofacies, with beds of ripple-laminated sand, is overlain by planar and trough cross-laminated gravelly sand, filling small erosional channels (Fig. 2, log 1.2 km). The lower contact to the ripple-laminated sand is delineated by a 1-cm-thick layer of white well-sorted fine sand that drapes the ripples.

Unit E is interpreted to be fluvial sediment, deposited in a river-dominated delta setting. Similar sediment bodies have been described by Reading (1986, p. 137), where small-scale coarsening upward sequences reflect the infilling of shallow lakes by small deltas. The occurrences of charcoal, twigs and logs suggests that woody plants were growing somewhere within the drainage area of the river that deposited the sediments. A sinestral mammoth rib and scapula were retrieved from the sediments, but were undiagnostic for species identification. There are no indications that the delta was deposited in a marine environment, so it may be a lacustrine deposit. Unit E does not contain *in situ* fossils that could indicate if it was deposited during interglacial or interstadial climate conditions.

Age control for units A–E

The age control for units A–E is based on AMS ^{14}C analyses on samples from units C and E, which give infinite ^{14}C ages. Moss and vascular detritus from unit C and three pieces of wood and a mammoth bone from unit E yielded ages of >40 kyr BP (Table 1 and Fig. 2), which provide some minimum limiting temporal constraints.

Optically stimulated luminescence dating was attempted on five sediment samples from the fluvial sands and silts of Unit E, with only partial success (Table 2; Fig. 2). A notable advantage of OSL dating is that luminescence is solar reset in seconds to minutes compared with hours for the same response from thermoluminescence (e.g. Godfrey-Smith *et al.*, 1988). Investigations on Svalbard demonstrate, for littoral and sublittoral environments, that most of the inherited OSL is solar reset with deposition and that any remaining OSL is within the analytical error when dating sediments that are $\geq 10^4$ years old (Forman, 1999). We used green-stimulated luminescence (GSL) on coarse-grained (150 to 200 μm) quartz on four samples using

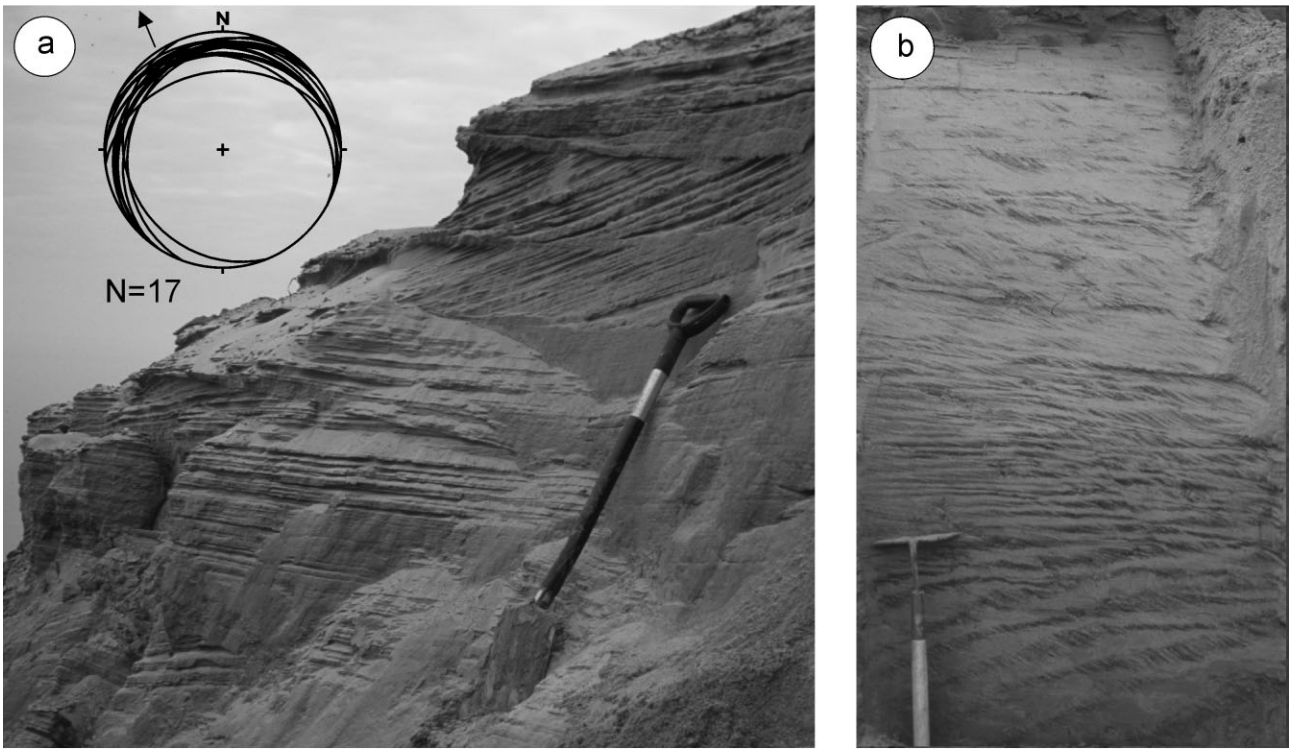

Figure 4 (a) Cross-stratified fluvial distributary channel sediments of unit E (at log 1.95 km), with erosional lower contacts of individual beds. The stereo net shows palaeocurrent directions given by orientations of cross-beds, $N = 17$. (b) Minor interdistributary bay sediments of unit E at log 1.2 km

Table 2 Green (GSL) and infrared (IRSL) stimulated luminescence data and ages for deltaic sediments, Cape Sphindler Sections, Yugorsky Peninsula, Russia

Laboratory number	UIC761[f]	UIC766[g]	UIC772[g]	UIC773[g]	UIC840[g]
Stratigraphic section (km)	1.95	1.2	1.2	1.2	1.95
Unit and elevation (m a.s.l.)	E/31.5	E/6	E/11	E/16	E/33.5
Excitation wavelength (nm)	880 ± 80	514 ± 20	514 ± 20	514 ± 20	514 ± 20
Alpha count (ks cm^{-2})[a]	0.18 ± 0.01	0.28 ± 0.02	0.18 ± 0.01	0.34 ± 0.02	0.26 ± 0.01
Th (ppm)	2.55 ± 0.35	3.23 ± 0.49	2.78 ± 0.35	4.04 ± 0.57	2.78 ± 0.43
U (ppm)	0.73 ± 0.12	1.31 ± 0.18	0.68 ± 0.13	1.53 ± 0.21	1.28 ± 0.16
Unsealed/sealed[b]	0.98 ± 0.07	1.00 ± 0.07	0.97 ± 0.07	1.07 ± 0.07	1.06 ± 0.07
K_2O (%)[c]	$1.00. \pm 0.02$	2.05 ± 0.02	0.97 ± 0.02	1.79 ± 0.02	2.40 ± 0.02
Dose rate (Gy/ka)[d]	1.11 ± 0.05	1.67 ± 0.10	0.96 ± 0.06	1.87 ± 0.11	1.94 ± 0.12
Equivalent dose (Gy)[e]	210.15 ± 0.86	$>200.44 \pm 3.86$	Saturated	$>261.03 \pm 12.08$	Saturated
OSL age (ka)	189.1 ± 19.6	$>120.1 \pm 12.6$	Non-calculable	$>139.7 \pm 14.6$	Non-calculable

[a] Thick-source alpha-count rate; U and Th concentrations calculated from alpha count rate, assuming secular equilibrium.
[b] The ratio of bulk alpha count rate under sealed and unsealed counting conditions. A ratio of >0.94 indicates little to none radon loss.
[c] Percentage potassium determined by ICP–MS on a homogenised 50 g aliquot by Activation Laboratories LTD, Ontario, Canada.
[d] Dose-rate includes a contribution from cosmic radiation of 0.13 ± 0.01 Gy kyr^{-1} and a moisture content of $40 \pm 10\%$, reflecting the saturated and frozen state of sandy sediments during burial.
[e] Errors for De determinations are determined using a non-linear least-squares routine, based upon the Levenburg-Marquarrdt (Press *et al.*, 1986, pp. 521–528.), in which inverse-variance weighted data are modelled by a saturating exponential function. Errors are generated for each De calculation in a variance–covariance matrix. The resulting uncertainties in De reflect dispersion in the data and random errors associated with modelling the dose response as a saturating exponential. The mean De and errors are evaluated from a range of individual Des for 2 to 90 s since light exposure. Standard statistical data-weighting procedures are utilised to calculate an average De and associated errors. All errors are at one sigma.
[f] OSL age determined on the fine-grained (4–11 μm) polymineral fraction by infrared excitation (880 ± 80 nm). Samples were excited for 90 s, and the resulting IRSL was recorded in 1-s increments. The IRSL was measured at least 1 day after preheating at 160°C for 5 h. The measured alpha efficiency factor of 0.03 ± 0.01 was used in age calculations.
[g] OSL age determined on the coarse-grained (150–200 μm) quartz fraction by green light excitation (514 ± 20 nm). Samples were excited for 90 s and the resulting GSL was recorded in 1-s increments. The GSLwas measured at least 1 day after preheating at 160°C for 5 h.

multiple aliquot additive dose procedures (Singhvi *et al.*, 1982). Quartz grains were isolated following modified procedures outlined in Stokes (1994) with inspection of quartz grain separates under an optical microscope with immersion oils to assess the purity of the separate through mineralogical point counts. The single aliquot regeneration technique (SAR; Murray and Wintle, 2000) for coarse-grained quartz was purposely avoided because of the suspected antiquity of samples (>100 ka) and the near saturation response to additive beta dose that would give apparently finite ages by SAR, although surely older (e.g. Forman and Pierson, 2000; Mangerud *et al.*, 2001). Two quartz separates (UIC772 and UIC840) showed insufficient growth in

luminescence (saturation) with additive beta dose to calculate an equivalent dose and thus did not yield ages (Table 2). Two other samples, UIC766 and UIC773, exhibited <150% rise in luminescence with an additive beta dose of >1 kGy yielding ages of ca. >120 ka and >140 ka, respectively, and these estimates are considered to be minimum estimates. Only one sample (UIC761) yielded sufficient fine-grained (4–11 μm) polymineral separate to be analysed by infrared stimulated luminescence (IRSL), which has been usefuel in dating late Quaternary near-shore marine deposits on Svalbard (Forman, 1999). This sediment yielded a distinct non-saturated response with a greater than fourfold increase in luminescence with additive beta dose of 3 kGy, which gave the finite age estimate of 189.1 ± 19.6 ka (UIC761). It is prudent to consider luminescence ages >100 ka to be possible minimum estimates because of uncertainties in the stability of trapped electrons over geological time and modelling of the luminescence growth curve near saturation (e.g. Mejdahl, 1988; Wintle *et al.*, 1993; Huntley *et al.*, 1996; Forman *et al.*, 2000).

Thus, we conclude that Unit E, situated between the two tills, probably pre-dates the Eemian and may be associated with non-glacial conditions during MOIS 7 or possibly earlier. Marine oxygen isotope stage 7 corresponds to Saale/Drenthe interstadial conditions in the Quaternary climatostratigraphy of northern Europe, 250–190 ka (Lowe and Walker, 1997, p. 11). De Jong (1988) described an early Saalian interstadial from The Netherlands, the Hoogeveen Interstadial, which he considered to have been relatively warm, and correlated to MOIS 7. One consequence of this is that unit D might have been deposited by a regional glaciation during MOIS 8, corresponding to the Drenthe glaciation in northern Europe, 300–250 ka (Lowe and Walker, 1997) and that units A–C are interglacial sediments of Holsteinian age (MOIS 9–11, >300 ka). This interpretation differs from that of Manley *et al.* (2001), who assigned units A–C an Eemian age (MOIS 5e), and the till and glacier ice, in this study assigned unit D, a Weichselian age.

Unit F: silty–clayey glacial diamicton

Unit F is a massive to weakly laminated silty–clayey diamicton, which occurs at 2.9 km and discontinuously between 1.0 and 0.6 km (Fig. 2, logs 2.9 km, 0.8 km and 0.6 km; Fig. 3). It is a 0.5 to 2 m thick unit with a sharp and unconformable lower contact. Underlying deposits are usually glaciotectonised. The diamicton is massive and contains millimetre to metre-scale lenses and pods of silt and sand in which many have been deformed into lenses and stringers of sorted silt and sand. At 1.0 km, three facies of unit F were recognised: a lowermost facies of a dense, massive clay, which grades into a heterogeneous clay with small stretched-out rafts and stringers of silt and fine sand; it is overlain by a lithofacies of sharply superimposed unconsolidated diamicton, with a concentration of bedrock clasts that are striated on lower surfaces. Striated clasts otherwise are rare in the unit, but a stone horizon was intermittently observed where unit F is absent and unit E intersects the surface (Fig. 3). Most of the stones are frost shattered, but some exhibit glacial striae, and are interpreted to be a lag horizon from unit F. Unlike the unit D glacial diamicton, unit F lacks mollusc valves and shell fragments.

The pervasively deformed lenses and pods of silt and sand are indicative of glacial shearing and we interpret unit F to be a subglacial diamicton. However, there is a lack of evidence for lodgement associated with this diamicton. This unit may be heavily contorted sediment brought in by an overflowing glacier and thus, a deformation till (Elson, 1989; Dreimanis, 1989; Hart and Boulton, 1991; Benn and Evans, 1998). Stone lags and the concentration of clasts in the looser, upper part of unit F may reflect material that escaped subglacial frictional deposition, and was melted out beneath a retreating ice-sheet or through mass wasting (cf. Krüger and Humlum, 1981; Van der Meer *et al.*, 1999). The unit F glacial diamicton was unrecognised by Manley *et al.* (2001).

Unit G: peat, sand and silt

The surficial deposit, unit G occurs along the top of the cliffs from 0.2 to 0.3 km, and from 2.5 to 2.9 km, forming an intermittent capping layer that fills local depressions and blankets older deposits (Fig. 3). It generally measures less than a metre in thickness, but is about 11 m thick at 2.6 km. Unit G contains peat, laminated silt and silty peat and massive fine sand and silt. Unit G was described by Manley *et al.* (2001) and Andreev *et al.* (2001) and interpreted to reflect a mosaic of post-glacial, terrestrial depositional environments, primarily shallow lacustrine and peatland settings, with minor aeolian, low-energy fluvial and colluvial deposition. Eighteen AMS ^{14}C dated plant macrofossils assign it an age range from ca. 12.8 to 0.8 kyr BP (Table 1; Andreev *et al.*, 2001; Manley *et al.*, 2001). Thus, this unit was deposited during the latest Pleistocene and Holocene and provides minimum limiting ages for the subjacent glacial diamictons.

Glaciotectonic deformation

Much of the stratigraphy at Cape Shpindler has been extensively deformed or displaced by the passage of an ice sheet or glacier. Below we present structural measurements and glaciotectonic descriptions from seven exposures that show the complexity of the glacier dynamic record. The structures are used to interpret former ice-movement directions. Furthermore, the glacial diamictons related to the structures are described in order to infer former subglacial conditions. Three of the exposures occur along the cross-section, two exposures are situated in a gully at 1.8 km and in the eastern wall of the thermocirque at 2.0 km (Figs 1c and 3), and two additional exposures occur east of the main cross section, at −2.55 km and at −2.6 km (Fig. 1c).

Exposure 2.0 km

Description

Enclosed within the glacier ice and diamicton of unit D are sharply delineated intraclasts of folded unit C sediments, with primary stratification barely discernible (Fig. 5a). These folds appear to be imbricated and overturned towards the south. The fold axis of one fold presented an orientation of 60 to 70°/20 to 30° (Fig. 5b). This fold occurs at a somewhat lower elevation than the rest of the observed folded intraclasts. It is therefore unknown if the fold is in its own stratigraphical position or an allochthon as are the rest of the observed folds in this section. The glacier ice of unit D1 is conformably overlain by a dense diamicton of unit D2, containing bullet shaped striated bedrock clasts, shell fragments and occasional whole paired shells.

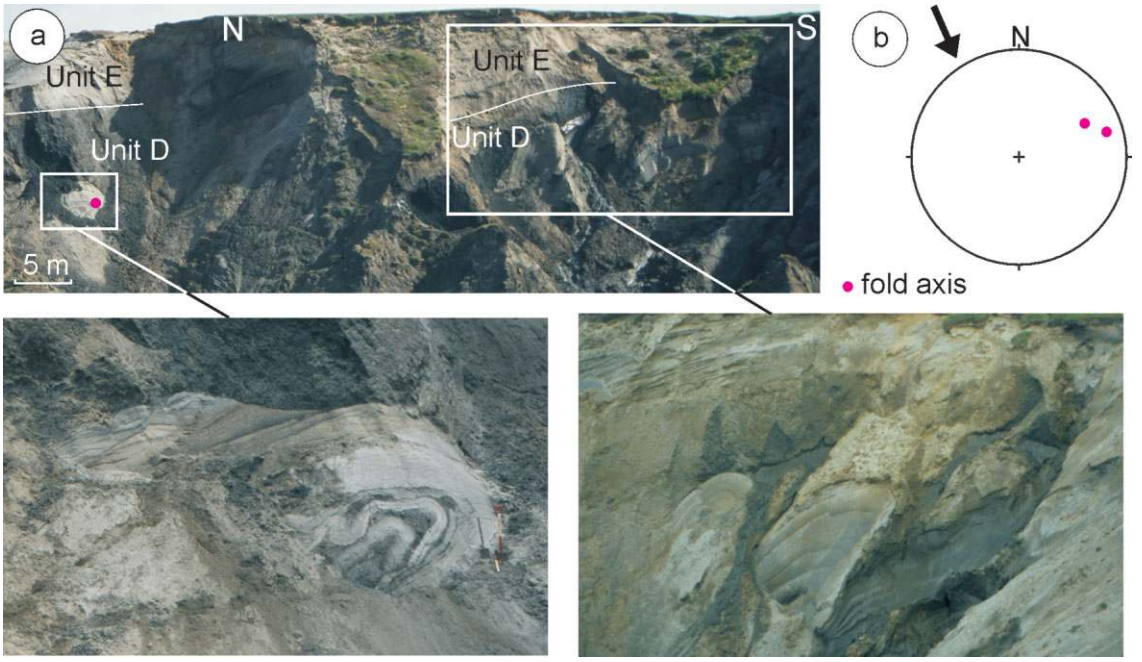

Figure 5 (a) Exposure in the eastern wall of the thermocirque at 2 km, showing folded intraclasts of sand within the relict glacial ice/diamicton complex; (b) stereogram showing the fold axis of the fold in the lower left picture and the direction of glacial transport, inferred from the fold axis and southward verging folds

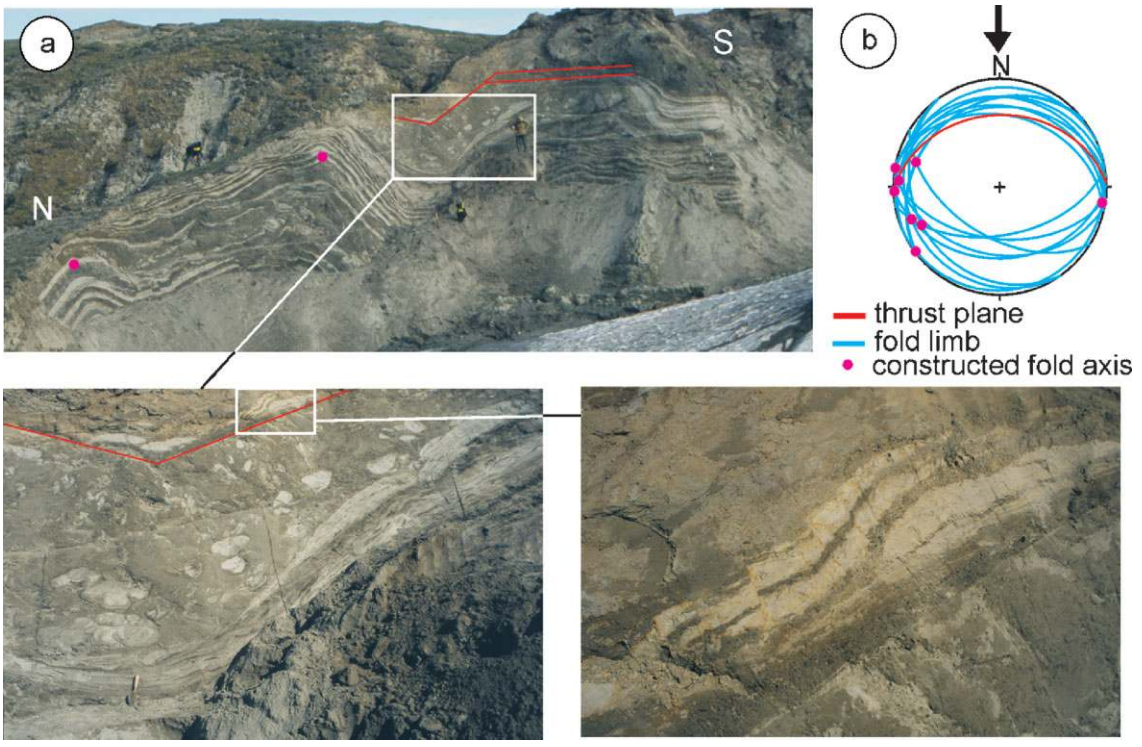

Figure 6 (a) Exposure in the gully at 1.8 km with folded and deformed unit C1 sediments. Note pods of silt and thrust plane in the lower left picture and the snake's head structure in the lower right picture; (b) Stereogram with inferred direction of glacial transport

Interpretation

The apparent preferred overturning of several folds towards the south, and measured ENE–WSW orientation of one fold axis, suggest a glacial push from the north-northwest (Fig. 5b). Because the folded intraclasts have sharp contacts with the surrounding glacier ice and primary stratification is discernible, the sediment was probably frozen when entrained by the advancing ice. Furthermore, ductile deformation within the intraclasts suggests high ice content, indicating at least partly frozen bed conditions. Apart from the intraclasts of folded sand within the glacial complex, the basal signature of the glacial diamicton and its sole superposition on relict glacier ice indicate transport of subglacial material to higher englacial positions.

Exposure 1.8 km

Description

A set of open folds in unit C1, with fold axes trending east to west, are slightly overturned towards the south (Fig. 6a). Their

antiformal fold hinges are progressively situated at higher elevations southwards, with a fold wavelength and amplitude approximately 7 to 10 m and 2 m, respectively. The uppermost beds of the southernmost fold, and the core of the northernmost antiform is broken up into boudins. Sediments overlying the boudins of the southernmost fold are pods of sand and silt within a finer matrix (Fig. 6a) and frequently showing extensive fissility. Many pods exhibit flat tops and some pods have augen-like forms. A thrust plane penetrates from south of the middle antiform and towards the southernmost antiform. The thrust plane strikes east to west and one measurement indicates a northward dip of 34° (Fig. 6b). It appears to have been folded. Imbricated elongated intraclasts of sand (snake's head structures), with a top to the south sense of movement, occur directly above the thrust plane (Fig. 6a). The glaciotectonised unit C1 beyond the southernmost antiform is overlain by the diamicton of unit D2.

Interpretation

The top-to the-south sense of movement of snake's head structures, as well as orientations of fold axes and shear planes, indicate a tectonic transport and ice movement direction from north to south (Fig. 6b). As the folds are rather open and only slightly inclined, we interpret the folding to have occurred proglacially (cf. Croot, 1987; Hambrey and Huddart, 1995; Asbjørn and Pedersen, 1996). The boudinage structures could suggest subglacial extensional conditions at some time during deformation. The pods of sand within a fissile, finer matrix are interpreted as a penetrative glaciotectonite with the coarser-grained pods acting as stiff or rigid regions within a more rapidly deforming fine-grained matrix (cf. Hart and Boulton, 1991; Benn and Evans, 1996).

Exposure 2.92 km

Description

Unit C1 is deformed into a drag fold with its fold axis trending approximately east to west (Fig. 7a). The contact to overlying diamicton, unit F, is an inclined (20°) thrust plane, striking approximately 65° (Fig. 7b). Unit C1 beneath the thrust plane displays no structures counteracting the shear direction of the thrust plane. Overlying till of unit F contains lenses of silt and sand.

Interpretation

Because the sediments beneath the drag fold are practically undeformed (Fig. 3), the possibility of backthrusting is excluded. Thus, the drag fold is interpreted to reflect primary glaciotectonic transport from the south-southeast (Fig. 7b).

Exposure 1.0 km

Description

Sandy beds of unit E show evidence of glaciotectonic deformation in the form of low-angle shear planes, small-scale diapirism and reverse faults (Fig. 8a). A shear plane, delineated by a gravel lag is orientated 321 to 348°/8 to 12° and a decimetre-scale reverse fault is oriented 130°/32° (Fig. 8b). All other measured shear planes strike approximately north to south and the diapirs appear slightly overturned towards the east. Primary structures are penetrated or replaced by glaciotectonic structures. The deformed unit C sediments are unconformably overlain by the deformation till of unit F. Imbricated, stretched out lenses of sand and silt in the upper part of the till indicate a top to the left (east) sense of movement (Fig. 8a).

Interpretation

Shear planes, the reverse fault and eastwards overturned diapirs indicate a greatest principal stress axis that is oriented west-southwest to east-northeast, and show eastward sense of movement, thus favouring a tectonic transport from the west-southwest (Fig. 8b). Using the terminology of Benn and Evans (1996), the deformation in the sandy sediments classify this as a penetrative glaciotectonite, although diapirs testify to local non-penetrative deformation. Because primary structures can hardly be seen, the deformed sandy sediments are interpreted as an intermediate form of deformation till and glaciotectonite, or it might be a deformation till that has undergone brittle shear (Benn and Evans, 1996).

Exposure 0.75 km

Description

A normal shear fault, with a considerable but unknown vertical displacement, occurs in the sand of unit C (Fig. 9a). The shear fault is orientated 308°/35° and the shearing has resulted in folding of the footwall sediments, where the fold axis strikes northwest to southeast (Fig. 9b). Smaller scale normal faults, antithetic to the main northeast-dipping normal fault, occur in the hanging wall (Fig. 9a). The structure is unconformably overlain by the till of unit F. In the gully at 0.76 km, orientated perpendicular to the coastal section, small-scale normal listric faults with apparent northward dips occur immediately below the contact with the till (Fig. 9a). These systematic faults, together with a small sigma structure in the lower part of the diamicton, indicate northward sense of movement.

Interpretation

The large scale normal fault and the smaller-scale listric normal faults could be indicative of extensional subglacial shear (cf. Croot, 1987; Asbjørn and Pedersen, 1996) imposed by a glacier advancing from the southwest (Fig. 9b). Furthermore, the homogenised nature of the overlying glacial diamicton, containing only mm-scale deformed lenses and beds of silt and sand, indicate a highly strained subglacial deformation till.

Exposure at −2.55 km

Description

In a section measuring approximately 30 m × 4 m, occurring below 5 m a.s.l., deformed strata of ripple-laminated sandy and silty sediments occur. Embedded in the sediments is a wedge of massive clay (Fig. 10a). The strata are unconformably overlain by undeformed, peaty stratified mud. Laminations and contacts between deformed beds within the disturbed strata

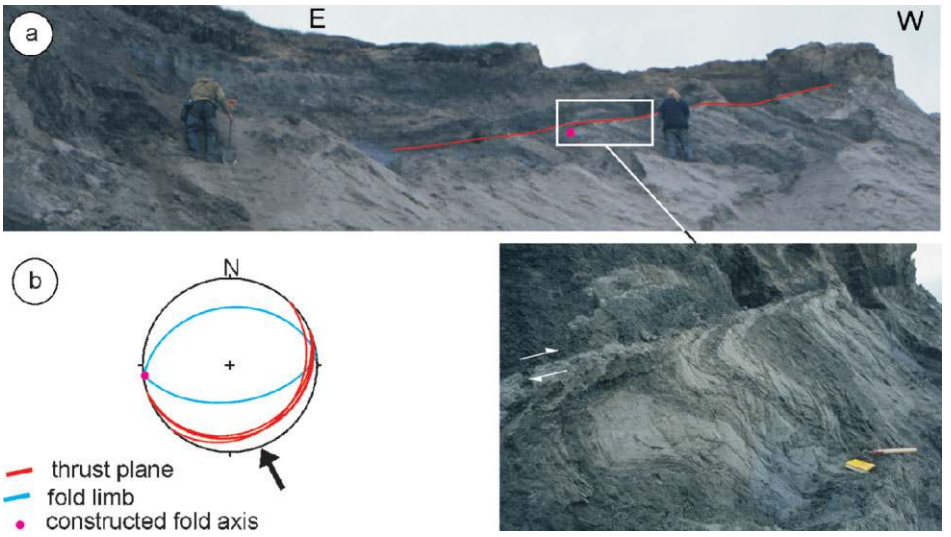

Figure 7 (a) Exposure at 2.9 km with unit C1 sediments deformed into a drag fold below a thrust fault and till of unit F; (b) stereogram with inferred direction of glacial transport

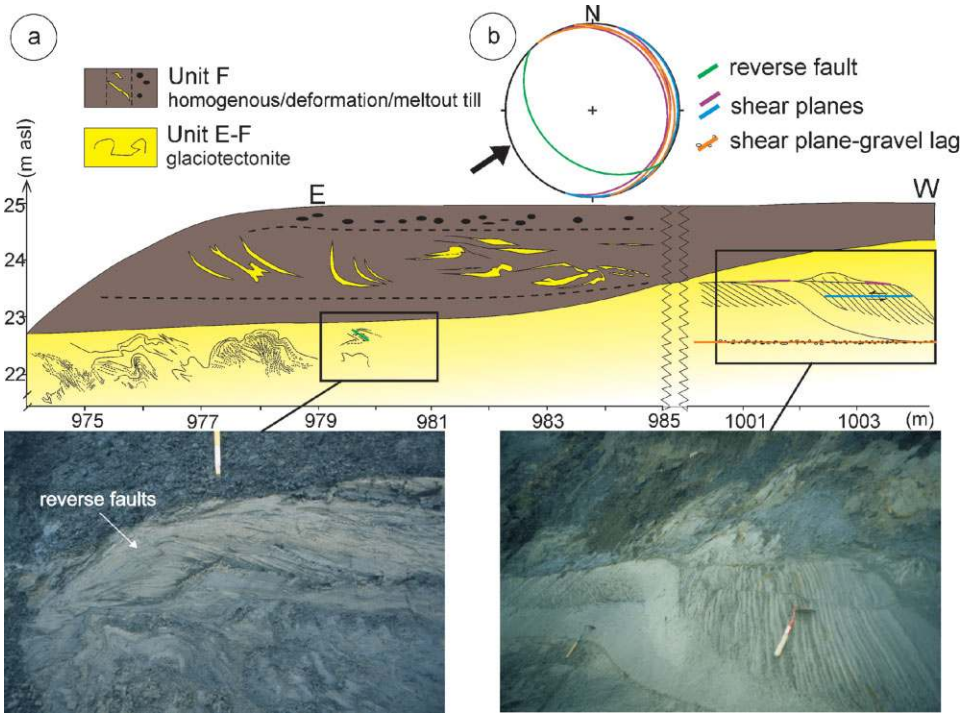

Figure 8 (a) Exposure at 1.0 km with diapirs, thrusts and a small-scale reverse fault. All structures have an apparent eastward sense of movement; (b) stereogram with inferred direction of glacial transport

strike 214° to 226° and dip 30° to 80° (Fig. 10b). Along some of these contacts occur sheared out pieces of clay (Fig. 10a), emanating from the main clay body, implying simple shear. One shear plane cuts reverse faults, and ripple lamination between this shear plane and the next is deformed into small, asymmetric folds overturned towards the west (Fig. 10a). Shear planes, reverse faults and overturned folds in the deformed ripple-laminated sand, show westward sense of movement.

Interpretation

The orientation of reverse faults and sense of movement shown by the shear planes and asymmetric folds suggest a deforming glacial push from the southeast (Fig. 10b).

Exposure at −2.6 km

Description

In the exposure at −2.6 km, tilted beds of gravel, sand and silt are sheared off along a shear zone in the upper part of the exposure (Fig. 11a). Ripple marks, indicating the way-up direction, define the structure as a syncline in the form of a drag fold. The fold axis trends approximately 60° (Fig. 11b). Smaller scale drag folds in gravel and overturned folds are present in the upper part of the exposure (Fig. 11a).

Interpretation

All structures in the exposure consistently suggest a deforming push from the southeast (Fig. 11b).

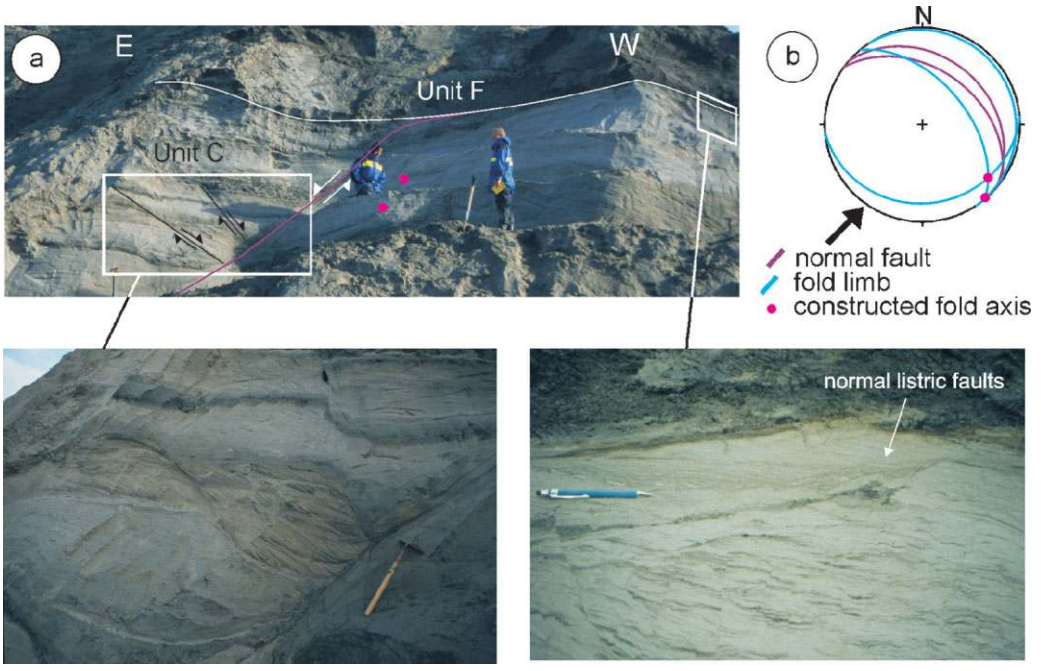

Figure 9 (a) Exposure at 0.75 km with the upper and lower left picture showing a normal shear fault (>10 m displacement) unconformably overlain by till of unit F and the lower right picture showing listric normal faults (above the pen); (b) stereogram with inferred direction of glacial transport

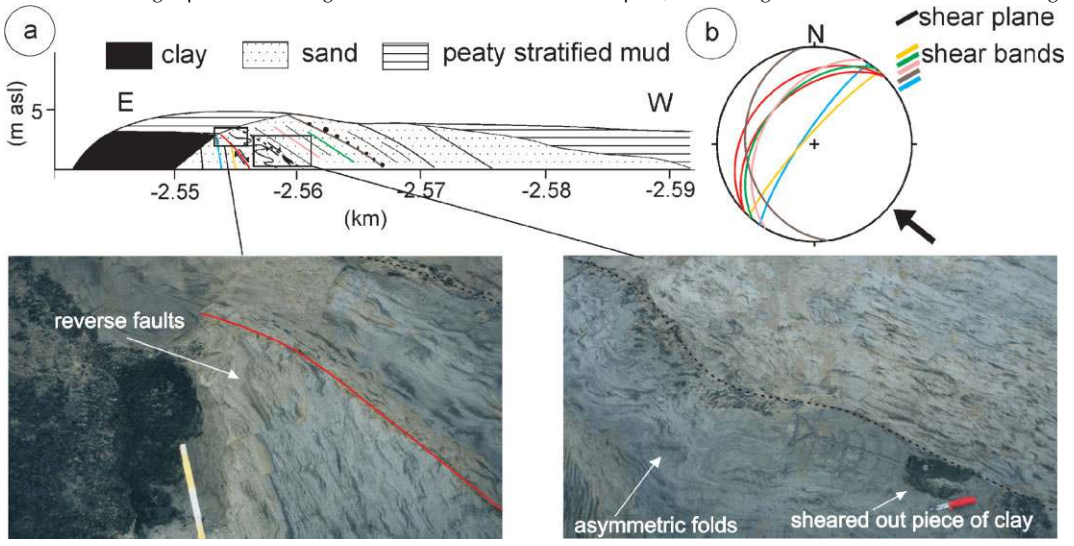

Figure 10 (a) Exposure at −2.55 km, showing a clay body, from where shear planes emanate. Note the sheared out piece of clay along one of the shear planes in the lower right picture; (b) stereogram with inferred direction of glacial transport

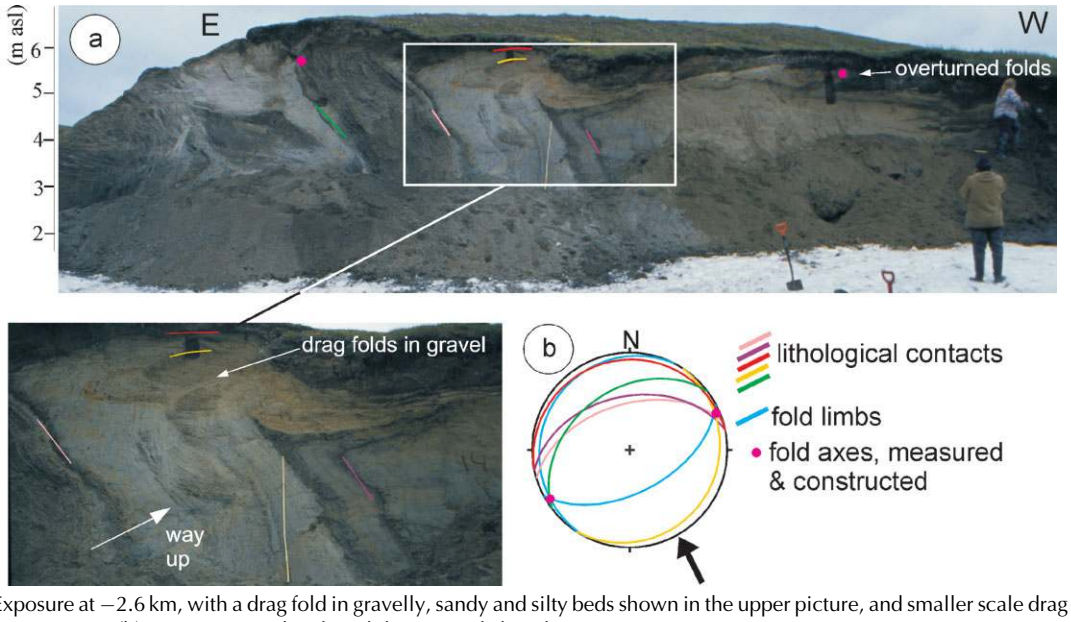

Figure 11 (a) Exposure at −2.6 km, with a drag fold in gravelly, sandy and silty beds shown in the upper picture, and smaller scale drag folds in gravel shown in the lower picture; (b) stereogram with inferred direction of glacial transport

Till genesis and basal conditions

Unit D2 contains striated clasts, is thicker and a finer grained glacial diamicton than unit F. In the thermocirque, where the glacier ice of subunit D1 occurs, the diamicton of subunit D2 is superimposed on unit D1, occasionally with a conformable contact. The diamicton was not found to occur below relict glacier ice. Furthermore, imbricated rafts of folded sand occur within both the glacier ice and the associated diamicton. Thus, we suggest that the glacier entrained frozen subglacial material; sand, marine clay and diamicton that was transported along thrust planes to a higher position in the ice (e.g. Moran *et al.*, 1980; Hambrey *et al.*, 1999). This diamicton is associated with melt-out processes with partly inherited properties of a primarily basally transported diamicton (Dreimanis, 1989). Although shearing can take place under cold-based glaciers (Echelmeyer and Zhongxiang, 1987; Tison *et al.*, 1993), the combination of striated, bullet shaped stones and subglacial rafts in the ice indicate an at least partly warm-based ice sheet (e.g. Weertman, 1961; Hooke, 1970). The ice sheet was probably thin near its terminus and periodically frozen to its bed. When the ice-front reached higher ground, the obstacle formed by both the ice frozen to its bed and the uphill movement, probably resulted in compression and high-angle thrusting. Overturned folds at 1.8 km testify to ductile deformation before shear resistance was overcome and the subglacial sediment was entrained into the ice. The thrust planes probably developed along weak planes in the frozen bed. Boudinage structures testify to later subglacial extensional strains. The glacial complex of unit D can be compared to the thrusted and contorted glacio-mixtures described from outcrops by the Yenisei River by Astakhov and Isayeva (1988) and Astakhov *et al.* (1996). There, subglacial processes reflect a dynamic sole where sliding of a cold-based glacier may have provoked subglacial extensional shearing in frozen fine-grained sediments and the development of englacial thrust planes within the ice during compression and deformation at an obstacle.

Overall, the till of unit F is slightly coarser grained than the till of unit D because it contains thin and discontinuous laminae of fine sand and silt in the otherwise clayey matrix. It only possesses clasts in its upper part, where it is also less consolidated. The lower contact is everywhere sharp and unconformable. The underlying sand and mud are deformed in both a brittle and ductile manner into a glaciotectonite (Banham, 1977; Pedersen, 1993; Benn and Evans, 1996). The observation that the underlying sand is sometimes deformed in a ductile manner could testify to high ice content during deposition and deformation, and thus indicate a largely cold-based glacier.

Conclusions and discussion

The stratigraphical and structural data from the Cape Shpindler coastal cliffs record two glacial events and three periods of ice-free conditions during the Late Quaternary (Fig. 12).

1 During interglacial conditions, a coarsening upwards sequence of marine to fluvial sediments (units A, B and C) was deposited in connection with progradation and/or marine regression from an interglacial highstand, possibly through glacio-isostatic compensation.
2 During an older glacial event, represented by the glacial complex of unit D, ice moved from an ice-divide somewhere to the north, probably on Novaya Zemlya, and advanced across the southern Kara Sea, overriding the interglacial/interstadial sediments. The ice later stagnated and was buried in glacial sediments. The glacial event is represented in the cliffs by bodies of buried glacier ice (unit D1), till (unit D2) and glaciotectonic disturbances.
3 Thereafter followed a period of fluvial deposition in a river-dominated lake delta (unit E). There is no conclusive evidence in the form of *in situ* fossils for warm climatic conditions, although woody plants were growing within the drainage area of the palaeo-river. Unit E could represent interglacial or interstadial conditions.
4 Later, the area was again subjected to glacial overriding. During this younger glacial event, ice moved from an ice divide inland, tentatively from the Pai-Hoi upland. It caused the deposition of unit F, and conspicuous glaciotectonic disturbances.
5 The uppermost stratigraphical unit in the cliffs, unit G, is largely Holocene (<12.5 kyr BP), comprising peats, aeolian, fluvial and lacustrine sediments.

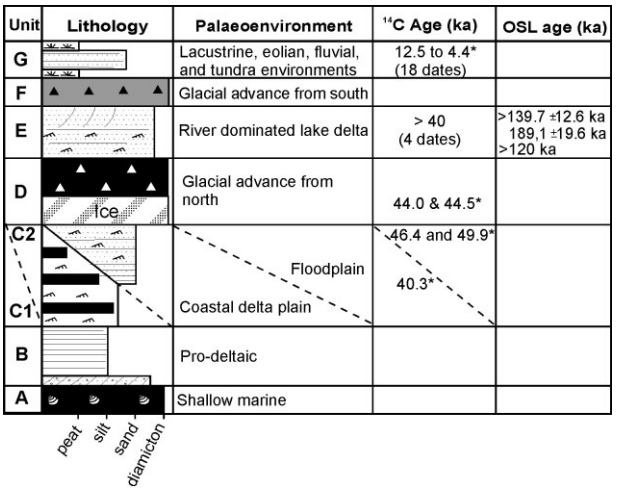

Figure 12 Composite stratigraphical log for the sediments exposed in the Cape Shpindler coastal sections: ∗, ages are from Manley *et al.* (2001)

The age-control for the Cape Shpindler sequence is not fully resolved and lacks good resolution: luminescence ages and AMS ^{14}C ages suggest that the older glacial event occurred prior to 120–200 ka and before 40 ka BP, respectively. Radiocarbon dates from unit G provide a minimum age for the younger glacial event, as being older than 12.5 kyr BP. Despite the paucity of luminescence dates to verify the proposed chronology for strata that is beyond the limits of ^{14}C dating, we choose to go with the limited chronological control that we have and regard the luminescence results as limiting minimum ages. Our chronology for the Cape Shpindler strata should therefore be regarded as tentative and needs further testing. Manley *et al.* (2001) suggested that units A, B, and C were interglacial sediments of Eemian (MOIS 5e) age. They based this conclusion on infinite AMS ^{14}C ages, molluscan faunal assemblages, stratigraphical position and similarity to Eemian transgressional sediments documented elsewhere across the Eurasian Arctic (Raukas, 1991; Astakhov, 1994). Sediments belonging to the Boreal Transgression, widely correlated with Eemian sediments of northwest Europe, are an important stratigraphical marker in coastal northern Russia, used for distinguishing between Weichselian (Valdaian) and older glacial deposits (see discussion in Astakhov, 2001; Houmark-Nielsen *et al.*, 2001). The three new luminescence dates from Cape Shpindler indicate that the interglacial sediments of units A,

B and C may be of Holsteinian (>300 ka) rather than of Eemian age. This also raises the possibility that interglacial sediments described from some other northern Russian and western Siberian sites, which in the absence of reliable chronologies have been correlated to the Boreal transgression and assigned Eemian age, might in some cases be considerably older? Marine sediments and tills containing fossils of warmer-than-present fauna, indicate that western Siberia has been affected by at least two 'Boreal' transgressions under interglacial conditions (Zubakov, 1972). The youngest marine strata with boreal molluscan fauna traditionally has been termed 'the Kasantzevo Formation' (Sachs, 1953) and correlated with the Eemian (Sukhorukova, 1998, 1999). Svendsen *et al.* (2001) suggested that several sequences traditionally ascribed to the Kazantsevo transgression might be considerably older. Our interpretation of the Cape Shpindler stratigraphy concurs with that view.

Another implication of the chronology is that the buried glacier ice (unit D1) and lower till (D2) might possibly have been deposited during the Drenthe glaciation, 300–250 ka (Lowe and Walker, 1997). Buried glacier ice, older than 40 ka, has been described from a number of sites in western Siberia (e.g. Kaplyanskaya and Tarnogrodsky, 1986; Astakhov and Isayeva, 1988; Gataullin, 1988; Astakhov *et al.*, 1996; Forman *et al.*, 1999). Most authors have suggested the buried glacier ice to be of Weichselian age, and Astakhov (1998) suggested that it was unlikely that buried glacier ice in western Siberia could have survived through the warm Eemian transgression. However, once glacier ice becomes incorporated in the permafrost and thawing slows down, glacier ice in such a position might survive for more than one interglacial. Much of the permafrost in Siberia is a relict of Pleistocene climate conditions (French, 1996, p. 56). Kudryavtsev *et al.* (1978) mapped the thickness of permafrost in the Yugorski Peninsula as being 200–400 m, implying that it is in disequilibrium with the present climate and could largely be relict. Huge bodies of glacier ice have survived through the Holocene without melting (Astakhov *et al.*, 1996), and could have survived previous interglacials as well. The present occurrence of subsea-shelf permafrost in the Kara Sea along western Yamal Peninsula (Kudryavtsev *et al.*, 1978) also illustrates the preservation potential of relict permafrost.

Most reconstructions of the Eurasian Ice Sheet depict a concentric continental-scale ice sheet, centred over the extensive shallow shelf areas of the Barents and Kara Seas and infringing on adjacent land areas (Lambeck, 1995; Rutter, 1995; Peltier, 1996; Astakhov *et al.*, 1999; Svendsen *et al.*, 1999; Tveranger *et al.*, 1999; Mangerud *et al.*, 2001; Siegert *et al.*, 2001). Recent studies of Late Quaternary environmental developments in western Siberia and northern Russia (Forman *et al.*, 1999; Mangerud *et al.*, 1999; Svendsen *et al.*, 1999) suggest that the Yamal and Yugorski Peninsulas were not covered by an Eurasian Kara Sea ice-sheet during the Last Glacial Maximum (20–18 ka), and that the last continental-scale glaciations of northern Russia and western Siberia occurred during the Early–Middle Weichselian, during the interval 90–50 ka. Mangerud *et al.* (2001) suggest that in the Pechora area, west of Yugorski Peninsula, there were two major Early–Middle Weichselian glaciations, at 90 and 60 ka, where ice advanced from an ice divide in the southern Barants Sea–Kara Sea on to land. They base their conclusion on OSL dating of subtill sediments in the Pechora Valley and of lacustrine sediments related to Lake Komi, but have not been able to stratigraphically verify two separate glacial advances. The last ice advance over Yamal Peninsula deposited the Kara diamicton over large parts of western Yamal Peninsula, south of 71°20′N (Gataullin, 1988). Large-scale (metre to kilometre scale) glaciotectonic deformation on western Yamal, associated with the deposition of the Kara till, uniformly reflect a deforming thrust from south towards north, in a direction from the Urals or Pai-Hoi uplands (Gataullin, 1988; Forman *et al.*, 1999; Forman *et al.*, 2002). These include numerous large (10 to 80 m) closed to isoclinal and recumbent to gently inclined folds. The folds are often strongly asymmetrical, with fold axes trending 100°–120° and uniform vergence towards north to northeast (Gataullin, 1988; Astakhov *et al.*, 1996; Forman *et al.*, 1999, 2002). Gataullin (1988), Astakhov (1979, 1992) and Astakhov *et al.* (1996) interpreted the stratigraphical and glaciotectonic data from western Yamal to show deformation resulting from push by an ice-lobe from the Kara Sea Ice Sheet, entering the Baidarata Bay from the northwest. We suggest the data are not compatible with an ice-lobe in Baidarata Bay, running from northwest to southeast, but instead propose that the last ice overriding western Yamal Peninsula correlates with the younger south to north directed glacial advance recorded in the Cape Shpindler sections, which reached at least 71°20′N. The age of the advance is constrained by a number of ^{14}C and luminescence dates from the Marresale section on western Yamal as being older than ca. 45 kyr BP, probably 90–60 ka (Forman *et al.*, 1999, 2002).

The Yugorski data, combined with structural data from western Yamal (Gataullin, 1988; Forman *et al.*, 1999, 2002), suggest that the Pai-Hoi uplands, at their maximum reaching 468 m a.s.l., acted as a glaciation nucleus centre at some time during the Early–Middle Weichselian glaciation (Fig. 13). This might have been a relatively small marginal dome, at the fringes of—and confluencing with—a larger ice sheet in the Kara Sea, or possibly an ice sheet separated, both in time and space, from a Kara Sea ice-sheet. Ice was dispersed from the Pai-Hoi uplands both towards the Polar Urals to the south-southeast and towards the north, across Baidarata Bay and onwards over western Yamal Peninsula. This interpretation is compatible with the observation of Astakhov (1979, 1992, 1997) and Astakhov *et al.* (1999) that the Polar Urals were not covered by any extensive ice-sheet during the last (Early–Middle Weichselian) glaciation, but were affected by ice-flow from the north. Glacial striae on Pai-Hoi, showing ice-movements from north to northeast across Yugorski Peninsula (see Astakhov *et al.* 1999, p. 27) could be remnants from an older glacial episode, possibly the glacial advance that deposited units D1 and D2 in the Cape Shpindler coastal cliffs. The Early–Middle Weichselian ice-cap on Pai-Hoi may have been largely cold-based, and thus older glacial striae were preserved.

This interpretation has some implications for the growth and configuration of the last Kara Sea Ice Sheet. To allow for the formation of a local ice cap on the Pai-Hoi uplands, the Kara Sea Ice Sheet probably was relatively thin in its marginal areas. According to a reconstruction by Tveranger *et al.* (1999) of the surface form of the southwestern sector of the Kara Sea Ice Sheet, it reached only about 500 m a.s.l. in the Pai-Hoi area. Glaciological modelling by Siegert *et al.* (2001) also suggests that an Early–Middle Weichselian Kara Sea Ice Sheet was no thicker than 250–500 m at the Yugorski Peninsula. The uplands of Pai-Hoi, which for the most part have an altitude of around 200 m a.s.l., but reach almost 500 m at the highest elevation (Figs 1c and 13), would have constituted a topographical obstacle for such a thin ice sheet. Astakhov *et al.* (1999) mapped the marginal formations of the last Kara Sea and Barents Sea ice-sheets, the Early–Middle Weichselian Marchida Line, in northern European Russia, from the Timan Ridge in the west to the east of the Polar Urals. We suggest that the Pai-Hoi ice-cap, rather than the Kara Sea Ice Sheet proper, formed some of the hummocky morainic

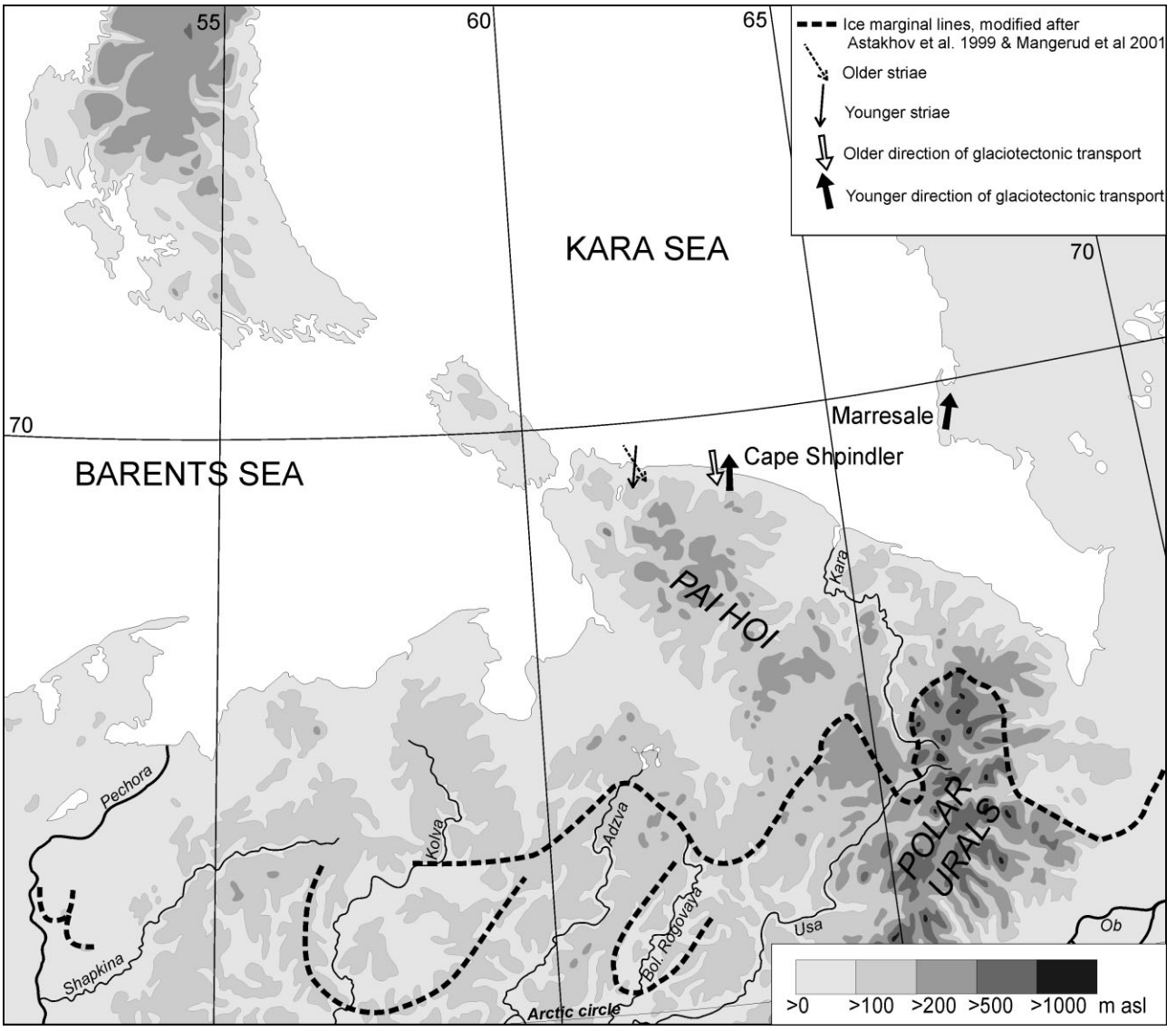

Figure 13 Topographic map of the Barents and Kara Sea region with directions of glacial movement as observed from glaciotectonic disturbances at Yamal and Yugorski Peninsula and glacial striae 35 km west of Cape Shpindler. The outline of morainic landforms modified after Astakhov *et al.* (1999) and Mangerud *et al.* (2001)

landscapes mapped by them on the southern fringes of the Yugorski Peninsula and the northern and western escarpment of the Polar Urals (Fig. 13).

During the past few years the extensive research initiative of Quaternary Environmental Eurasian North (QUEEN) (Svendsen *et al.*, 1999; Thiede *et al.*, 2001; Svendsen *et al.*, 2001) has not only clarified a number of questions concerning the temporal and spatial distribution of Late Quaternary glaciations in Eurasia and adjoining shelf areas, but also identified several cases of enigmatic regional glaciation and ice flow patterns (Astakhov *et al.*, 1999; Mangerud *et al.*, 1999; Alexanderson *et al.*, 2001; Houmark-Nielsen *et al.*, 2001; Kjær *et al.*, 2001). Did local ice domes, centred on the mainland ridges and highlands, grow and interact with the larger Barents–Kara Sea ice-sheet at some point during the Early–Middle Weichselian, and did the highland areas bordering the Kara Sea act as ice-sheet nucleation areas during the Early–Middle Weischselian glaciations? We propose that the glacial fingerprinting on Yugorski Peninsula (this study) and western Yamal Peninsula (Forman *et al.*, 1999, 2002) better conforms with such a scenario rather than reflecting a predominantly single concentric, continental-scale Barents–Kara Sea ice-sheet.

Acknowledgements We express our gratitude to the following people and institutions for various support: Valery Gataullin contributed to the project and fieldwork with his vast experience of stratigraphical work in western Siberia; Björn Magnor contributed with his knowledge in structural geology during the fieldwork; Torbjörn Andersson, Torbjörn Persson and Per Samuelsson assisted in the fieldwork; Svend Funder identified the molluscan fauna, and Marit Solveig Sidenkrantz identified the foraminiferd fauna. Lennart Björklund critically scrutinised the glaciotectonic documentation, descriptions and interpretations. The Swedish Natural Sciences Research Council has generously supported the project (grants to Ó. Ingólfsson). The Swedish Polar Research Secretariat provided logistic support. Marina Leibman and the Earth Cryosphere Institute of the Russian Academy of Sciences participated in the fieldwork and assisted in the logistics. All IRSL dates and AMS ^{14}C dates were financed by grants from YMER. The manuscript benefited from critical reviews by C. Hjort and J. I. Svendsen.

References

Alexanderson H, Hjort C, Møller P, Antonov O, Pavlov M. 2001. The North Taimyr ice-marginal zone, Arctic Siberia—a preliminary overview and dating. *Global and Planetary Change* **31**: 427–445.

Andreev AA, Manley WF, Ingólfsson Ó, Forman SL. 2001. Environmental changes on Yugorski Peninsula, Kara Sea, Russia, during the last 12 800 radiocarbon years. *Global and Planetary Change* **31**: 255–264.

Asbjørn S, Pedersen SAS. 1996. Progressive glaciotectonic deformation in Weichselian and Palaeogene deposits at Feggeklint, northern Denmark. *Bulletin of Geological Society of Denmark* **42**: 153–174.

Arkhipov SA, Bespaly VG, Faustova MA, Glushkova OYu, Isayeva LL, Velichko AA. 1986. Ice sheet reconstructions. *Quaternary Science Reviews* **5**: 475–482.

Astakhov VI. 1979. New data on the latest activity of Kara shelf glaciers in West Siberia. *IGCP Project 73/1/24, Quaternary Glaciations in the Northern Hemisphere, Report 5*. Prague; 22–31.

Astakhov VI. 1992. The last glaciation in West Siberia. *Sveriges Geologiska Undersökning, Serie Ca* **81**: 21–30.

Astakhov VI. 1994. *The Last Glaciation in Russia's European Arctic*. Report 13/94, Centre for Studies of Environment and Resources, University of Bergen; 81 pp.

Astakhov VI. 1997. Late glacial events in the central Russian Arctic. *Quaternary International* **41/42**: 17–25.

Astakhov VI. 1998. The last ice sheet of the Kara Sea: terrestrial constraints on its age. *Quaternary International* **45/46**: 19–28.

Astakhov VI. 2001. The stratigraphic framework for the Upper Pleistocene of the glaciated Russian Arctic: changing paradigms. *Global and Planetary Change* **31**: 283–295.

Astakhov VI, Isayeva LL. 1988. The 'Ice hill': an example of 'retarded deglaciation' in Siberia. *Quaternary Science Reviews* **7**: 29–40.

Astakhov VI, Kaplyanskaya FA, Tarnogradsky VD. 1996. Pleistocene permafrost of West Siberia as a deformable glacier bed. *Permafrost and Periglacial Processes* **7**: 165–191.

Astakhov VI, Svendsen JI, Matiouchkov A, Mangerud J, Maslenikova O, Tveranger J. 1999. Marginal formations of the last Kara and Barents ice sheets in northern European Russia. *Boreas* **28**: 23–45.

Banham PH. 1977. Glaciotectonites in till stratigraphy. *Boreas* **6**: 101–105.

Benn DI, Evans DJA. 1996. The interpretation and classification of subglacially deformed materials. *Quaternary Science Reviews* **15**: 23–52.

Benn DI, Evans DJA. 1998. *Glaciers and Glaciation*. Edward Arnold: London.

Croot DG. 1987. Glacio-tectonic structures: a mesoscale model of thin-skinned thrust sheets? *Journal of structural Geology* **9**: 797–808.

De Jong J. 1988. Climatic variability during the past three million years, as indicated by vegetational evolution in Northwest Europe and with emphasis on data from The Netherlands. *Philosophical Transactions of the Royal Society of London, Series B* **318**: 603–617.

Dreimanis A. 1989. Tills: their genetic terminology and classification. In *Genetic Classification of Glacigenic Deposits*, Goldthwait RP, Match CL (eds). A. A. Balkema: Rotterdam; 17–83.

Elson JA. 1989. Comment on glaciotectonite, deformation till, and comminution till. In *Genetic Classification of Glacigenic Deposits*, Goldthwait RP, Match CL (eds). A. A. Balkema: Rotterdam; 85–88.

Echelmeyer K, Zhongxiang W. 1987. Direct observation of basal sliding and deformation of basal drift at sub-freezing temperatures. *Journal of Glaciology* **33**: 83–98.

Forman SL. 1999. Infrared and red stimulated luminescence dating of late Quaternary near-shore sediments from Spitsbergen, Svalbard. *Arctic, Antarctic, and Alpine Research* **31**(1): 34–49.

Forman SL, Pierson J. 2000. Optically-stimulated luminescence dating of known age eolian deposits: tests of accuracy and precision. *Geological Society of America, Abstracts with Program*, at http://rock.geosociety.org/absindex/annual/2000/51084.htm.

Forman SL, Ingólfsson Ó, Gataullin V, Manley WF, Lokrantz H. 1999. Late Quaternary stratigraphy of western Yamal Peninsula, Russia: new constraints on the configuration of the Eurasian Ice sheet. *Geology* **27**: 807–810.

Forman SL, Pierson J, Lepper K. 2000. Luminescence geochronology. In *Quaternary Geochronology: Methods and Applications*, Sowers JM, Noller JS, Lettis WR (eds). American Geophysical Union Reference Shelf 4: Washington, DC; 157–176.

Forman SL, Ingólfsson Ó, Gataullin V, Manley WF, Lokrantz H. 2002. Late Quaternary stratigraphy, glacial limits and paleoenvironments of the Marresale area, western Yamal Peninsula, Russia. *Quaternary Research* **57**: 355–370.

French HM. 1996. *The Periglacial Environment*. Longman: Harlow.

French HM, Harry DG. 1990. Observations on buried glacier ice and massive segregated ice, western Arctic Coast, Canada. *Permafrost and Periglacial Processes* **1**: 31–43.

Gataullin V. 1988. *Upper Quaternary deposits of the western coast of Yamal Peninsula*. PhD Thesis, All-Russian Geological Institute: St Petersburg; 213 pp. (In Russian.)

Godfrey-Smith DI, Huntley DJ, Chen W-H. 1988. Optical dating studies of quartz and feldspar sediment extracts. *Quaternary Science Reviews* **7**: 373–380.

Goldfarb JI, Ezhova AB, Romanjuk BF. 1985. Northwestern coast of the Yugorsky Peninsula (Shpindler site). In *Investigation of Geotechnical Conditions of Some Oil and Gas Perspective Areas of the Kara Sea*, Vol. 1 Part 2, Valpeter AP, Goldfarb JI, Gataullin V (eds). VNII Morego: Riga, Latvia; 71–136. (In Russian.)

Hambrey MJ, Huddart D. 1995. Englacial and proglacial glaciotectonic processes at the snout of a thermally complex glacier in Svalbard. *Journal of Quaternary Science* **10**: 313–326.

Hambrey MJ, Bennet MR, Dowdeswell JA, Glasser NF, Huddart D. 1999. Debris entrainment and transfer in polythermal valley glaciers. *Journal of Glaciology* **45**: 69–86.

Hart J, Boulton GS. 1991. The interrelation of glaciotectonic and glaciodepositional processes within the glacial environment. *Quaternary Science Reviews* **10**: 335–350.

Hooke RL. 1970. Morphology of the ice-sheet margin near Thule, Greenland. *Journal of Glaciology* **9**: 303–324.

Houmark-Nielsen M, Demidov I, Funder S, Grøsfjeld K, Kjær K, Larsen E, Lavrova N, Lysså A, Nielsen JK. 2001. Early and Middle Valdaian glaciations, ice-dammed lakes and periglacial interstadials in northwest Russia: new evidence from the Pyoza River area. *Global and Planetary Change* **31**: 215–237.

Huntley DJ, Short MA, Dunphy K. 1996. Deep traps in quartz and their use for optical dating. *Canadian Journal of Physics* **74**(3–4): 81–91.

Kaplayanskaya FA, Tarnogradsky VD. 1986. Remnants of the Pleistocene ice sheets in the permafrost zone as object for paleoglaciological research. *Polar Geography and Geology* **10**: 257–265.

Kjær K, Demidov I, Houmark-Nielsen M, Larsen E. 2001. Distinguishing between tills from Valdaian ice sheets in the Arkhangelsk region, Northwest Russia. *Global and Planetary Change* **31**: 201–214.

Krüger J, Humlun O. 1981. The proglacial area of Mýrdalsjökull. *Folia Geographica Danica* **15**: 58.

Kudryavtsev VA, Kondratyeva KA, Romanovski NN. 1978. Zonal and regional patterns of formation of the permafrost region in the USSR. In *Proceedings, 3rd International Conference on Permafrost*, Vol. 1. National Research Council of Canada: Ottowa; 419–426.

Lambeck K. 1995. Constraints on the Late Weichselian ice sheet over the Barents Sea from raised shorelines. *Quaternary Science Reviews* **14**: 1–16.

Lowe JJ, Walker MJC. 1997. *Reconstructing Quaternary Environments*. Longman Group: Harlow.

Mahaney WC, Michel FA, Solomatin VI, Hütt G. 1995. Late Quaternary stratigraphy and soils of Gydan, Yamal and Taz Peninsula, northwestern Siberia. *Palaeogeography, Palaeoclimatology, Palaeoecology* **113**: 249–266.

Mangerud J, Svendsen JI, Astakhov VI. 1999. Age and extent of the Barents and Kara ice sheets in northern European Russia. *Boreas* **28**: 46–80.

Mangerud J, Astakhov VI, Murray A, Svendsen JI. 2001. The chronology of a large ice-dammed lake and the Barents–Kara Ice Sheet advances, Northern Russia. *Global and Planetary Change* **31**: 321–336.

Manley WF, Lokrantz H, Gataullin V, Ingólfsson Ó, Andersson T, Forman SL. 2001. Late Quaternary stratigraphy, radiocarbon chronology, and glacial history at Cape Shpindler, southern Kara sea, Arctic Russia. *Global and Planetary Change* **31**: 239–254.

Mejdahl V. 1988. The plateau method for dating partially bleached sediments by thermo-luminescence. *Quaternary Science Reviews* **7**: 347–348.

Michel FA. 1998. The relationship of massive ground ice and the Late Pleistocene history of northwest Siberia. *Quaternary International* **45/46**: 43–48.

Moran SR, Clayton L, Hooke RLB, Fenton MM, Andriashek LD. 1980. Glacier-bed landforms of the prairie region of North America. *Journal of Glaciology* **25**(93): 457–476.

Murray AS, Wintle AG. 2000. Luminescence dating of quartz using an improved single-aliquot regenerative-dose protocol. *Radiation Measurements* **32**(1): 57–73.

Pedersen SAA. 1993. The glaciodynamic event and glaciodynamic sequence. In *Glaciotectonics and Mapping Glacial Deposits*, Aber JS (ed.). *Canadian Plains Proceedings* **25**: 67–85.

Peltier WR. 1996. Mantle viscosity and ice-age ice sheet topography. *Science* **273**: 1359–1364.

Press WH, Flannery BP, Teukolsky SA, Vetterling WT. 1986. *Numerical Recipes: The Art of Scientific Computing*. Cambridge University Press: Cambridge.

Raukas A. 1991. Eemian interglacial record in the northwestern European part of the Soviet Union. *Quaternary International* **10–12**: 183–189.

Reading HG. 1986. *Sedimentary Facies and Environments*. Blackwell Scientific Publications: Oxford.

Reineck HE, Singh IB. 1975. *Depositional Sedimentary Environments*. Springer-Verlag: New York.

Rutter N. 1995. Problematic ice sheets. *Quaternary International* **28**: 19–37.

Sachs VN. 1953. *The Quaternary Period in the Soviet Arctic*. Leningrad-Moscow; 627 pp. (In Russian.)

Siegert MJ, Dowdeswell JA, Hald M, Svendsen JI. 2001. Modelling the Eurasian Ice Sheet through a full (Weichselian) glacial cycle. *Global and Planetary Change* **31**: 367–385.

Singhvi AK, Sharma YP, Agrawal DP. 1982. Thermoluminescence dating of dune sands in Rajasthan, India. *Nature* **295**: 313–315.

Stokes S. 1994. *Optical dating of selected Late Quaternary aeolian sediments from the southwestern United States*. Unpublished PhD thesis, University of Oxford: Oxford.

Sukhorukova SS. 1998. The key sequence of marine sediments and climate fluctuations of the Kazantsevo (Eemian) interglacial (northern Siberia). *Geologia i Geofizika* **39**: 74–84. (In Russian.)

Sukhorukova SS. 1999. Late Pleistocene palaeogeography of North-West Siberia. *Antropozoikum* **23**: 37–42.

Svendsen JI, Astakhov VI, Bolshiyanov DYu, Demidov I, Dowdeswell JA, Gataullin V, Hjort C, Hubberten HW, Larsen E, Mangerud J, Melles M, Möller P, Saarnisto M, Siegert MJ. 1999. Maximum extent of the Eurasian ice sheets in the Barents Sea region during the Weichselian. *Boreas* **28**: 234–242.

Svendsen JI, Alexanderson H, Astakhov V, Demidov I, Dowdeswell JA, Gataullin V, Henriksen M, Hjort C, Houmark-Nielsen M, Hubberten HW, Jakobsson M, Kjær K, Larsen E, Lumkka JP, Lysså A, Mangerud J, Maslenikova O, Matioushkov A, Möller P, Raab A, Saarnisto M, Siegert M, Wischer F. 2001. The Late Quaternary glacial history of northern Eurasia. In *Eurasian Ice Sheets. Final Report 1998–2000, Part B: Final Scientific Report*, Svendsen JE (ed.). University of Bergen: Bergen; 139–210.

Thiede J, Bauch HA, Hjort C, Mangerud J. 2001. Editorial: The Late Quaternary stratigraphy and environments of northern Eurasia and the adjacent Arctic seas—new contributions from QUEEN. *Global and Planetary Change* **31**: vii–x.

Tison JL, Petit JR, Barnola JM, Mahaney WC. 1993. Debris entrainment at the ice–bedrock interface in subfreezing temperature conditions. *Journal of Glaciology* **39**: 303–315.

Tveranger J, Astakhov VI, Mangerud J, Svendsen JI. 1999. Surface form of the south-western sector of the last Kara Sea Ice sheet. *Boreas* **28**: 81–91.

Van der Meer JJM, Kjær KH, Krüger J. 1999. Subglacial water-escape structures and till structures, Sléttujökull, Iceland. *Journal of Quaternary Science* **14**: 191–205.

Weertman J. 1961. Mechanism for the formation of inner moraines found near the edge of cold icecaps and ice sheets. *Journal of Glaciology* **3**: 965–978.

Wintle AG, Questiaux DG, Roberts RG, Spooner NA. 1993. Dating loess up to 800 ka by thermoluminescence—comment. *Geology* **21**(6): 568–568.

Zubakov VA. 1972. *Recent Sediments of the West Siberian Lowland*. Leningrad; 312 pp. (In Russian.)